IEEE Access
Multidisciplinary | Rapid Review | Open Access Journal

Received February 2, 2019, accepted March 26, 2019, date of publication April 9, 2019, date of current version December 31, 2019.

Digital Object Identifier 10.1109/ACCESS.2019.2909981

Fuzzy Region-Based Active Contours Driven by Weighting Global and Local Fitting Energy

JIANGXIONG FANG[1,2], HUAXIANG LIU[2], LITING ZHANG[2], JUN LIU[2], AND HESHENG LIU[1]

[1]School of Mechanical and Electrical Engineering, Nanchang University, Nanchang 330031, China
[2]School of Geophysics and Measure Control Technology, East China University of Technology, Nanchang 330013, China

Corresponding authors: Jiangxiong Fang (fangchj2002@163.com) and Hesheng Liu (hsliu@vip.163.com)

This work was supported in part by the National Natural Science Foundation of China under Grant 61463005, Grant 61866001, Grant 21664002, and Grant 61463017, in part by the China Postdoctoral Science Foundation under Grant 2017M612163, in part by the Natural Science Foundation of Jiangxi Province under Grant 20181BAB211017 and Grant 20171BAB202028, in part by the Jiangxi Provincial Key Laboratory of Digital Land under Grant DLLJ201804, and in part by the Science and Technology Project of Jiangxi Provincial Department of Education under Grant GJJ170450 and Grant GJJ160539.

ABSTRACT Active contour model (ACM) has been a successful method for image segmentation. The existing ACMs poorly segment the images with intensity inhomogeneity or non-homogeneity, and the results highly depend on the initial position of the contour. To overcome these disadvantages, we proposed a fuzzy region-based active contour driven by weighting global and local fitting energy, wherein we propose a fuzzy region energy with local spatial image information, which has been proved convex and ensures the segmentation results independent of initialization, to motivate an initial evolving curve of pseudo level set function (LSF), followed by the pseudo LSF and further smoothed by an edge energy to accurately extract the object boundaries and maintain its distance feature. In addition, in the fuzzy region energy, instead of using the Euler-Lagrange equation to minimize the energy functional, we develop a more direct method to calculate the change of the fuzzy region energy. The experimental results on synthetic and real images with high noise and intensity inhomogeneity show that the proposed model can obtain better performance than the state-of-the-art active contour models, and takes less running time. The code is available at: https://github.com/fangchj2002/FRAGL.

INDEX TERMS Active contour, intensity inhomogeneity, edge energy, fuzzy region energy.

I. INTRODUCTION

Image segmentation is an elementary task in the field of image processing and widely used in image analysis, computer vision, medical imaging, etc. [1]. Its aim is to divide a given image into several regions where each region is homogeneous with regard to a certain characteristic, i.e. intensity, color, texture [2]. Many image segmentation algorithms [3] have designed for different applications. Among these algorithms, active contour model (ACM) [4]–[6] is one of the most effective image segmentation algorithms. Its advantage is that the model can deal with topological changes of contour curves. In these ACMs, the evolving contour is represented as the zero level set and driven towards object boundaries by minimizing the energy functional.

Generally, the existing ACMs are categorized into two classes: edge-based ACMs and region-based ACMs. In the edge-based ACMs [4]–[5], gradient information is used to guide the evolving contour to move toward the object boundaries. But it is sensitive to the initial contours. Different from the edge-based ACMs, the region-based ACMs [6]–[8] utilize the global image information to drive the motion of the evolving contours. Many image features, such as intensity, color, texture, are incorporated into the region-based energy functional. In the region-based ACMs, a zero level set function (LSF) is used to express the contour curve, also called signed distance function. The Chan-Vese model [6] based on Mumford-Shah (M-S) model [8] is a most widely used region-based ACM. It makes use of the difference between the inside and outside average intensities to drive the motion of the evolving curve instead of image gradient. But the model poorly deals with intensity inhomogeneity and its non-convex energy function with the regularization term makes the evolving curves stuck in local optima. In addition, its periodical re-initialization of the LSF greatly increases computational cost.

The associate editor coordinating the review of this manuscript and approving it for publication was Sunil Karamchandani.

It is a challenging task to development a robust region-based ACM to segment the images with severe intensity inhomogeneity. Many improved Chan-Vese models [9]–[23] are proposed by incorporating local image information into the energy functional. Vese and Chan [9] proposed a piecewise smooth (PS) model and extended it to multiphase image segmentation using two LSFs. But its computational cost is very high. Li et al. [10], [11] proposed a local binary fitting (LBF) model with a localized convolutional kernel function to extract local image information. To extract image features, it utilizes a scalable parameter with spatially varying weight and local image information to control the evolution curve. They further proposed a distance regularized level set evolution (DRLSE) model [12], [13] to eliminate the periodical re-initialization of LSF by introducing a penalty term, which can smooth the LSF and maintain the distance feature during the curve evolution. A local image fitting (LIF) model [14] is constructed based on a fitted image with local image information to approximate the input image. In the LIF model, a Gaussian filter is used to smooth the LSF and maintain the characteristic of the LSF during the curve evolving. Many improved fitted energy-based models are constructed to deal with intensity inhomogeneity, e. g. local hybrid image fitting energy (LHIF) model [15], local likelihood image fitting (LLIF) energy model [16], and local cosine fitting energy [17]. An active contour model driven by local pre-fitting energy (LPE) [18] is formulated based on the average image intensities in local region before the evolution of curve. The LPE model costs less running time, but it is impossible to adaptively extract the object local features. Local statistical region-based ACM [19]–[22] based on the Chan-Vese model via Gaussian function is introduced to formulate the energy function. A variational model [23] is proposed to handle intensity inhomogeneity with the multiplicative noise. However, these models cannot obtain good results for highly noisy and intensity inhomogeneity images.

Non-convex energy function in the region-based ACMs makes the evolving contour stuck in local optima and causes the segmentation results sensitive to the initial conditions. To solve this problem, a fuzzy energy-based active contour (FEBAC) [24] is proposed by incorporating fuzzy sets into ACM. Later on, many improved FEBAC model are proposed. The global and local FEBAC model (GL-FEBAC) [25]–[27] is constructed by incorporating both local spatial and intensity information into ACM, which can decrease the effect of intensity inhomogeneity in given images. Image feature, such as kernel metric, [28], and shape prior [29], is also fused into the FEBAC model to improve the segmentation performance. However, these models without the regularization term lead to the non-smoothness of the evolving curve and cannot maintain the distance feature of the pseudo LSF. In additions, updating the degree of membership by computing the change of pixel-by-pixel energy function in each iteration greatly increases computational cost.

In this study, we proposed a novel Fuzzy Region-based Active contour model with weighting Global and Local fitting energy for image segmentation, called FRAGL. The FRAGL model includes two parts. In the first part, a fuzzy region energy is formulated by constructing a weighting hybrid fitting energy with local spatial image information to approximate the image with intensity inhomogeneity. The energy functional has been proved strictly convex, which makes the result independent of initial conditions. Then, a more direct method is developed to compute the difference between the new and old energy energies to update the pseudo LSF. In the second part, an edge energy with a regularization term and a penalty term is designed to accurately detect object boundaries. The segmentation results on synthetic and real images with severe intensity inhomogeneity show that the proposed model can obtain better performance and take less running time compared with the popular region-based ACMs. Our main contributions are as follows:

1) The fuzzy region energy based on weighting local spatial information is constructed to reduce effect of intensity inhomogeneity in given images. Meanwhile, to accurately extract the object boundaries and maintain the distance feature of the pseudo LSF, an edge energy with a regularization term and a penalty term is designed.

2) The fuzzy region energy has been proved strictly convex, which ensures the segmentation results independent of initialization.

3) Instead of the Euler-Lagrange equations to solve the fuzzy region energy, which has slow convergence, a direct method, which computes the difference between the new and old energies to update the pseudo LSF for the whole image domain at a time, is developed and faster than the FBEAC model.

The remainder of this paper is organized as follows. Related work is described in Section 2. Section 3 describes the proposed model, including the fuzzy region energy, the edge energy, numerical approximation, and the algorithm of the detailed description steps. Section 4 depicts the experimental results including experimental results on synthetic and real images, robustness to initialization, comparison with the popular region-based ACMs, and effect of parameters. Finally, the conclusion is given in Section 5.

II. RELATED WORK

A. CHAN-VESE MODEL

Let $I(x) : \Omega \rightarrow R^d$ be a segmented image in the image domain Ω, where d is the dimension of the vector $I(x)$. Specially $d = 1$ defines the gray images while $d = 3$ denotes color images. The energy functional is defined as:

$$E^{CV}(C, c_1, c_2) = \mu \cdot len(C) + \lambda_1 \int_{Out(C)} (I(x) - c_1)^2 \, dx + \lambda_2 \int_{In(C)} (I(x) - c_2)^2 \, dx \quad (1)$$

where λ_1, λ_2 and μ are three positive constants, $Len(C)$ is the length of the contour C, $In(C)$ and $Out(C)$ denote two regions inside C and outside C, respectively, and its corresponding average intensities are c_1 and c_2.

To minimize the energy, a zero level set based on the Lipschitz function $\varphi(x)$ is used to express the contour curve C. The LSF $\varphi(x)$ is defined as follows:

$$\begin{cases} \phi(x) > 0 & if\ x \in In(C) \\ \phi(x) = 0 & if\ x \in On(C) \\ \phi(x) < 0 & if\ x \in Out(C) \end{cases} \tag{2}$$

Therefore, the energy functional $E^{CV}(C, c_1, c_2)$ defined in (1) is expressed as:

$$E_{\varepsilon}^{CV}(c_1, c_2, \phi) = \mu \cdot \int_{\Omega} \delta_{\varepsilon}(\phi) |\nabla\phi| \, dx + \lambda_1 \int_{\Omega} (I(x) - c_1)^2 \times H_{\varepsilon}(\phi) dx + \lambda_2 \int_{\Omega} (I(x) - c_2)^2 (1 - H_{\varepsilon}(\phi)) dx \tag{3}$$

where $H_{\varepsilon}(x) = 1/2 \cdot \lceil 1 + 2/\pi \cdot \arctan(x/\varepsilon) \rceil$ is the Heaviside function, $\delta_{\varepsilon}(x) = dH_{\varepsilon}(x)/dx$ is the Dirac delta function, where ε is a small positive constant.

Then, the variational method using the Euler-Lagrange equation is used to minimize the energy E^{CV} and the gradient descent algorithm is used to update the LSF. However, the Chan-Vese model cannot accurately handle the detection of objects for the images with intensity inhomogeneity.

B. LBF MODEL

Li et al. [9] proposed a local binary fitting (LBF) model by incorporating local image information, which is implemented by a Gaussian kernel function, to deal with intensity inhomogeneity in images. The energy functional in the LBF model is written as:

$$E^{LBF}(\phi, f_1, f_2) = \sum_{i=1}^{2} \lambda_i \int_{\Omega} \int_{\Omega} K_r(x - y) (I(y) - f_i(x))^2 \times H_i(\phi) dy dx + \mu \int_{\Omega} |\nabla H(\phi(x))| dx \tag{4}$$

where λ_i is positive constant, K_r is a Gaussian kernel function with standard deviation r, y is a spatial pixel independent of x, two smooth functions f_1 and f_2 are used to estimate the local intensities inside and outside the contour C, respectively.

The energy function by adding a penalizing term can avoid the re-initialization procedure and extract the desirable object(s) from the intensity inhomogeneous image. But the model still needs four convolution operators in every iteration, which increases the computational cost. In additions, the segmentation results are highly dependent on the initial localization.

C. FEBAC MODEL

To obtain global convex energy function, Krinidis and Chatzis [24] proposed a FBEAC model by incorporating the fuzzy sets into ACM. Different from the popular ACMs, the FEBAC model uses 0.5 level set as the evolving curve. The pseudo LSF is defined as:

$$\begin{cases} u(x) = 0.5 & I(x) \in C \\ u(x) > 0.5 & I(x) \in In(C) \\ u(x) < 0.5 & I(x) \in out(C) \end{cases} \tag{5}$$

where $I(x)$ is an input image, and $In(C)$ and $Out(C)$ denote the regions inside and outside the contour curve C, respectively.

By introducing the pseudo LSF defined in (5), which divides an input image into two regions, the energy function is expressed as:

$$E(C, c_1, c_2) = \eta \cdot Len(C) + \lambda_1 \int_{\Omega} [u(x)]^m (I(x) - c_1)^2 dx + \lambda_2 \int_{\Omega} [1 - u(x)]^m (I(x) - c_2)^2 dx \tag{6}$$

where the constants $\eta \geq 0$, $\lambda_1, \lambda_2 \geq 0$ are three fixed parameters, c_1 and c_2 are average intensities inside and outside the contour C, respectively, and m is an exponent. Two average intensities are defined as:

$$c_1 = \frac{\int_{\Omega} u(x)^m I(x) dx}{\int_{\Omega} u(x)^m dx}, \quad c_2 = \frac{\int_{\Omega} [1 - u(x)]^m I(x) dx}{\int_{\Omega} [1 - u(x)]^m dx} \tag{7}$$

To obtain the updating variable, keeping the parameters c_1 and c_2 fixed and minimizing the energy function $E(C, c_1, c_2)$ in (6) with respect to u, the degree of member-ship $u(x)$ can be obtained as follows:

$$u(x) = \frac{1}{1 + \left(\frac{\lambda_1 (I(x) - c_1)^2}{\lambda_2 (I(x) - c_2)^2} \right)^{\frac{1}{m-1}}}. \tag{8}$$

Specifically, in the computing process, the first step is to calculate the fuzzy membership for a certain pixel x in the image using (8). Then, the new fuzzy membership is updated according to the change of the energy function ΔE caused by the change of the fuzzy membership. If the value ΔE is negative, then the fuzzy membership is updated. Otherwise, the old one is kept. In the third step, the above process is repeated for the whole image domain, and one iteration is finished. Finally, the iterative process continues until the total energy is unchanged.

III. THE FRAGL MODEL

In this section, we will describe the FRAGL model in detail. Similar to the FEBAC model [24], the evolving contour C expressed as a 0.5 level set function defined in (5) separates the image domain Ω into two regions: object region and background region. The object and background regions are expressed as the inside region $C_{in}(u > 0.5)$ and outside region $C_{out}(u < 0.5)$, respectively. The FRAGL model F including the fuzzy region energy F^{fr} and the edge energy F^{edg} is written as:

$$F(u) = F^{fr}(u, g) + F^{edg}(u) \tag{9}$$

where g is an edge detector to reduce the image noise and smooth the image edge, which is defined as follows:

$$g(x) = \frac{1}{1 + |\nabla G_\sigma * I(x)|^2} \tag{10}$$

where ∇ is gradient operator of the input image $I(x)$, and G_σ is a Gaussian kernel with standard deviation σ.

A. FUZZY REGION ENERGY

The images in real world usually appear intensity inhomogeneity which causes blurred edges between adjacent regions. The formulation describing intensity inhomogeneity is usually written as:

$$I(x) = b(x)J(x) + n(x) \tag{11}$$

where $I(x)$ is an intensity value of the observed image, $b(x)$ is a smoothly changing bias field which reflects intensity inhomogeneity, $J(x)$ is a real intensity value of the inhomogeneity-free image, and $n(x)$ is additive noise. The additive noise $n(x)$ exists in various types including Gaussian noise, salt and pepper noise and speckle noise during imaging. To overcome the disadvantages, a region descriptor is used to eliminate the effects of intensity inhomogeneity. Or rather, a local region with spatial information is used to approximate the observed image with intensity inhomogeneity.

Let $\Omega \in R^d$ be the image domain, where d is the dimension of the vector $I(x)$, point x be a pixel in the image domain Ω, and point y be independent of point x and a neighborhood point centered at pixel x in a small rectangle or circle region $\Omega_x \subset \Omega$. Two average intensities f_o and f_b respectively corresponding to the inside (object) and outside (background) regions in local image domain Ω_x are defined as:

$$\begin{cases} f_o = mean(I(y)|y \in \Omega_x \cap u(y) > 0.5) \\ f_b = mean(I(y)|y \in \Omega_x \cap u(y) < 0.5) \end{cases} \tag{12}$$

where $u(y) \in [0, 1]$ is the fuzzy membership function in the local image domain Ω_x. In this paper, we design a local spatial weight $\omega(x, y)$ for pixel y

$$\omega(x, y) = \frac{1}{1 + dis(x, y)} \tag{13}$$

where $dis(x, y)$ denotes the spatial distance between pixel x and pixel y, the size of a local window is $(2k+1)\times(2k+1)$, the constant k called as the radius of the local window is a positive constant. Thus, two constants f_o and f_b can be represented as:

$$f_o = \frac{\int_\Omega \int_{\Omega_x} \omega(x, y) I(x)[u(x)]^m dy dx}{\int_\Omega \int_{\Omega_x} \omega(x, y)[u(x)]^m dy dx} \tag{14}$$

$$f_b = \frac{\int_\Omega \int_{\Omega_x} \omega(x, y) I(x)[1 - u(x)]^m dy dx}{\int_\Omega \int_{\Omega_x} \omega(x, y)[1 - u(x)]^m dy dx} \tag{15}$$

By filtering with local spatial windows, two constants f_o and f_b can be considered as the local average intensities inside and outside the contour C, respectively. When the evolving curves reach the exact boundary, the average prototypes of the inside and outside regions in the input image can be taken as $I_{in}^{fr} = \alpha f_o + \beta c_1$ and $I_{out}^{fr} = \alpha f_b + \beta c_2$, respectively, where α and β are two weighted constants and satisfy $\alpha + \beta = 1$. If the image contains more high intensity inhomogeneity, a larger value α is chosen. Otherwise, a smaller value α is chosen.

From the above analysis, the fuzzy region term F^{fr} with the fuzzy set [24] is given as follows:

$$\begin{aligned} F^{fr}(u, g) = \lambda_1 \int_\Omega [u(x)]^m g\,(I(x) - (\alpha f_o + \beta c_1))^2\, dx \\ + \lambda_2 \int_\Omega [1 - u(x)]^m g\,(I(x) - (\alpha f_b + \beta c_2))^2\, dx \end{aligned} \tag{16}$$

where λ_1 and λ_2 are positive weighted parameters, m is the weighting exponent on each fuzzy membership.

To compute the pseudo LSF $u(x)$, keeping the variables f_s, f_b, c_1, and c_2 fixed and calculating the minimization of the energy in (14) w. r. t u, we have:

$$\begin{aligned} &\lambda_1 \int_\Omega [u(x)]^m g\,(I(x) - (\alpha f_o + \beta c_1))^2\, dx \\ &+ \lambda_2 \int_\Omega [1 - u(x)]^m g\,(I(x) - (\alpha f_b + \beta c_2))^2\, dx = 0 \end{aligned} \tag{17}$$

The membership function $u(x)$ can be presented as:

$$u(x) = \frac{1}{1 + \left(\frac{\lambda_1 (I(x) - (\alpha f_o + \beta c_1))^2}{\lambda_2 (I(x) - (\alpha f_b + \beta c_2))^2}\right)^{\frac{1}{m-1}}} \tag{18}$$

B. EDGE ENERGY

To obtain the precise positioning of the object boundary and smooth the pseudo LSF, we designed an edge energy F^{edg} consisting of a regularization term and a penalty term. The edge energy is defined as:

$$F^{edg}(u) = l_1 L(u - 0.5) + l_2 P(u - 0.5) \tag{19}$$

where l_1 and l_2 are positive parameters, the first term called as the regularization term is the length of evolving contour to ensure the smoothness of the pseudo LSF, and the second term called as penalty term is to keep the consistency between the signed distance function and the pseudo LSF, and we have:

$$L(u = 0.5) = \int_\Omega \delta(u - 0.5)\, |\nabla(u - 0.5)| dx \tag{20}$$

$$P(u = 0.5) = \frac{1}{2} \int_\Omega (1 - |\nabla(u - 0.5)|)^2 dx \tag{21}$$

where ∇ denotes the Hamilton operator and $(\nabla\varphi)_{x,y} = \left(\frac{\partial\varphi}{\partial x}, \frac{\partial\varphi}{\partial y}\right)$ is the gradient of $\varphi = u - 0.5$.

C. NUMERICAL APPROXIMATION

The usual method to minimize the energy function in the region-based ACMs is the gradient descent optimizer based on the Euler-Lagrange equation. But its convergence speed is very slow. Inspired by the FEBAC model [24], we directly calculate the difference between the new and old energies

to update the pseudo LSF. If the changed value is negative, the new one is replaced. Otherwise, the old value is unchanged. It is straightforward that the global minima of the energy functional can easily obtain in an iterative way if the energy functional defined in (16) is convex. Therefore, we first prove the proposed energy functional is convex (***Appendix A***).

Let P be a given point in the image domain Ω, its corresponding intensity value and the degree of member-ship be $I_0 \in I(x)$ and u_0, respectively, and the fuzzy region energy be F^{fr}. Correspondingly, for the same point P, the constants c_1, c_2, f_o, and f_b become four new ones: $\hat{c}_1, \hat{c}_2, \hat{f}_o$, and $\hat{f}_b$, and the new total energy is $\hat{F}^{fr}$ when the new degree of membership at is u_{n}. The process of computing the difference $\Delta F^{fr} = \hat{F}^{fr} - F^{fr}$ between the old and new energies is presented in ***Appendix B***. Thus, the change of the energy function is given as follows:

$$\begin{aligned}
\Delta F &= \hat{F}^{fr} - F^{fr} = \left(\hat{F}_A^{fr} + \hat{F}_B^{fr}\right) - \left(F_A^{fr} + F_B^{fr}\right) \\
&= gt_1 \left(\alpha \frac{\omega(x,y) * \Delta u_1}{\omega(x,y) * (t_1 + \Delta u_1)} (I_0 - f_o) \right. \\
&\quad \left. + \beta \frac{\Delta u_1}{t_1 + \Delta u_1} (I_0 - c_1)\right)^2 \\
&\quad + gt_2 \left(\alpha \frac{\omega(x,y) * \Delta u_2}{\omega(x,y) * (t_2 + \Delta u_2)} (I_0 - f_b) \right. \\
&\quad \left. + \beta \frac{\Delta u_2}{t_1 + \Delta u_1} (I_0 - c_2)\right)^2 \\
&\quad + g\Delta u_1 \left(\frac{\alpha\omega(x,y) * t_1}{\omega_\sigma(x,y) * (t_1 + \Delta u_1)} (I_0 - f_o) \right. \\
&\quad \left. + \frac{\beta t_1}{t_1 + \Delta u_1} (I_0 - c_1)\right)^2 \\
&\quad + g\Delta u_2 \left(\frac{\alpha\omega(x,y) * t_2}{\omega(x,y) * (t_2 + \Delta u_2)} (I_0 - f_b) \right. \\
&\quad \left. + \frac{\beta t_2}{t_2 + \Delta u_2} (I_0 - c_2)\right)^2 \qquad (22)
\end{aligned}$$

where $t_1 = \sum_\Omega [u(x)]^m$, $\Delta u_1 = u_n^m - u_0^m$, $t_2 = \sum_\Omega [1 - u(x)]^m$, and $\Delta u_2 = (1 - u_n)^m - (1 - u_0)^m$.

From above, for pixel x, we can use (22) to compute the change of the energy functional. In the whole image domain Ω, let the degree of memberships $u(x)$ before and after updating respectively be $u_0(x)$ and $u_n(x)$, the change value of the energy be $\Delta F(x)$, so we have $u_0(x) = \sum_\Omega u_0$, $u_n(x) = \sum_\Omega u_n$, and $I(x) = \sum_\Omega I_0$. The change of the energy function $\Delta F(x)$ can be written as:

$$\begin{aligned}
\Delta F(x) &= \sum\nolimits_\Omega \Delta F \\
&= g \sum\nolimits_\Omega t_1 \left(\alpha \frac{\omega_\sigma(x,y) * \Delta u_1}{\omega_\sigma(x,y) * (t_1 + \Delta u_1)} (I_0 - f_o) \right. \\
&\quad \left. + \beta \frac{\Delta u_1}{t_1 + \Delta u_1} (I_0 - c_1)\right)^2 \\
&\quad + g \sum\nolimits_\Omega t_2 \left(\alpha \frac{\omega(x,y) * \Delta u_2}{\omega(x,y) * (t_2 + \Delta u_2)} (I_0 - f_b) \right. \\
&\quad \left. + \beta \frac{\Delta u_2}{t_1 + \Delta u_1} (I_0 - c_2)\right)^2 \\
&\quad + g \sum\nolimits_\Omega \Delta u_1 \left(\frac{\alpha\omega(x,y) * t_1}{\omega(x,y) * (t_1 + \Delta u_1)} (I_0 - f_o) \right. \\
&\quad \left. + \frac{\beta t_1}{t_1 + \Delta u_1} (I_0 - c_1)\right)^2 \\
&\quad + g \sum\nolimits_\Omega \Delta u_2 \left(\frac{\alpha\omega(x,y) * t_2}{\omega(x,y) * (t_2 + \Delta u_2)} (I_0 - f_b) \right. \\
&\quad \left. + \frac{\beta t_2}{t_2 + \Delta u_2} (I_0 - c_2)\right)^2 \\
&= gt_1 \left(\alpha \frac{\omega(x,y) * \Delta u_1(x)}{\omega(x,y) * (t_1 + \Delta u_1(x))} (I(x) - f_o) \right. \\
&\quad \left. + \beta \frac{\Delta u_1}{t_1 + \Delta u_1} (I(x) - c_1)\right)^2 \\
&\quad + gt_2 \left(\alpha \frac{\omega(x,y) * \Delta u_2(x)}{\omega(x,y) * (t_2 + \Delta u_2(x))} (I(x) - f_b) \right. \\
&\quad \left. + \beta \frac{\Delta u_2}{t_1 + \Delta u_1} (I(x) - c_2)\right)^2 \\
&\quad + g\Delta u_1(x) \left(\frac{\alpha\omega(x,y) * t_1}{\omega(x,y) * (t_1 + \Delta u_1(x))} (I(x) - f_o) \right. \\
&\quad \left. + \frac{\beta t_1}{t_1 + \Delta u_1(x)} (I(x) - c_1)\right)^2 \\
&\quad + g\Delta u_2(x) \left(\frac{\alpha\omega(x,y) * t_2}{\omega(x,y) * (t_2 + \Delta u_2(x))} (I(x) - f_b) \right. \\
&\quad \left. + \frac{\beta t_2}{t_2 + \Delta u_2(x)} (I(x) - c_2)\right)^2 \qquad (23)
\end{aligned}$$

where $\Delta u_1(x) = u_n^m(x) - u_0^m(x)$ and $\Delta u_2(x) = (1 - u_n(x))^m - (1 - u_0(x))^m$.

From the above computing process, unlike the FEBAC model [24], which calculates the alterations of the energies for each pixel at a time and needs large computation, we directly update the pseudo LSF of the whole image domain at a time by computing the difference between the old and new energies.

In the process of computing the edge energy, we calculate the derivative in (19) with regard to u, which is written as:

$$\begin{aligned}
\frac{\partial F^{edg}}{\partial u} &= l_1 \delta_\varepsilon (u - 0.5) div \left(\frac{\nabla(u - 0.5)}{|\nabla(u - 0.5)|}\right) \\
&\quad + l_2 \left(\nabla^2 (u - 0.5) - div \left(\frac{\nabla(u - 0.5)}{|\nabla(u - 0.5)|}\right)\right) \qquad (24)
\end{aligned}$$

In this paper, two weighting constants l_1 and l_2 are set to 1.

D. DESCRIPTION OF ALGORITHM STEPS

The computation step of the FRAGL model is described as follows:

1. Specify an input image, and initial parameters: weighting constants $\lambda_1, \lambda_2, \alpha, \beta, l_1$ and l_2, the maximum number of iterations *IterNum*, the radius of the local window k, and the edge detector matrix g.
2. Initialize pseudo LSF: set $u_0(x) > 0.5$ for one part, and $u_0(x) < 0.5$ for the other.
3. Compute the initial averages using (7) and (13): c_1, c_2, f_o, and f_b.
4. Update parameters: the degree of membership $u(x)$ using (16), the new constants $\hat{c}_1, \hat{c}_2, \hat{f}_o$ and $\hat{f}_b$ using (7) and (14)-(15).
5. Compute the difference between the new and old energies $\Delta F(x)$ using (23) in the whole image domain Ω. For point $x \in \Omega$, if the following equation $\Delta F(x)$ is negative, then replace $u_0(x)$ with $u_n(x)$; otherwise, keep the old value $u_0(x)$.

$$
\begin{aligned}
\Delta F(x) = gt_1 \Bigg(& \alpha \frac{\omega(x,y) * \Delta u_1(x)}{\omega(x,y) * (t_1 + \Delta u_1(x))} (I(x) - f_o) \\
& + \beta \frac{\Delta u_1}{t_1 + \Delta u_1} (I(x) - c_1) \Bigg)^2 \\
& + gt_2 \Bigg(\alpha \frac{\omega(x,y) * \Delta u_2(x)}{\omega(x,y) * (t_2 + \Delta u_2(x))} (I(x) - f_b) \\
& + \beta \frac{\Delta u_2}{t_2 + \Delta u_2} (I(x) - c_2) \Bigg)^2 \\
& + g\Delta u_1(x) \Bigg(\frac{\alpha\omega(x,y) * t_1}{\omega(x,y) * (t_1 + \Delta u_1(x))} (I(x) - f_o) \\
& + \frac{\beta t_1}{t_1 + \Delta u_1(x)} (I(x) - c_1) \Bigg)^2 \\
& + g\Delta u_2(x) \Bigg(\frac{\alpha\omega(x,y) * t_2}{\omega(x,y) * (t_2 + \Delta u_2(x))} (I(x) - f_b) \\
& + \frac{\beta t_2}{t_2} + \Delta u_2(x)(I(x) - c_2) \Bigg)^2
\end{aligned}
$$

where $\Delta u_1(x) = u_n^m(x) - u_0^m(x)$ and $\Delta u_2(x) = (1 - u_n(x))^m - (1 - u_0(x))^m$.

6. Regularize and smooth the pseudo LSF using the edge energy in (24).
7. Repeat steps 3-6 till the iterations are finished.

IV. EXPERIMENTS AND RESULTS

In this section, we test the segmentation performance of the proposed model on the synthetic and real images. Unless otherwise specified, some default parameters are set as follows: the pseudo LSF $u(x) = 0.7$ and $u(x) = 0.3$ respectively corresponding to the inside and outside regions, $m = 2$, the radius of the local weighting window $k = 5$, and the maximal number of iteration $IterNum = 100$. The experiments are processed using a 3.2-GHzIntel 4-core PC computer with 3GB of memory using the Matlab programming language. The code is available at the website: https://github.com/fangchj2002/FRAGL.

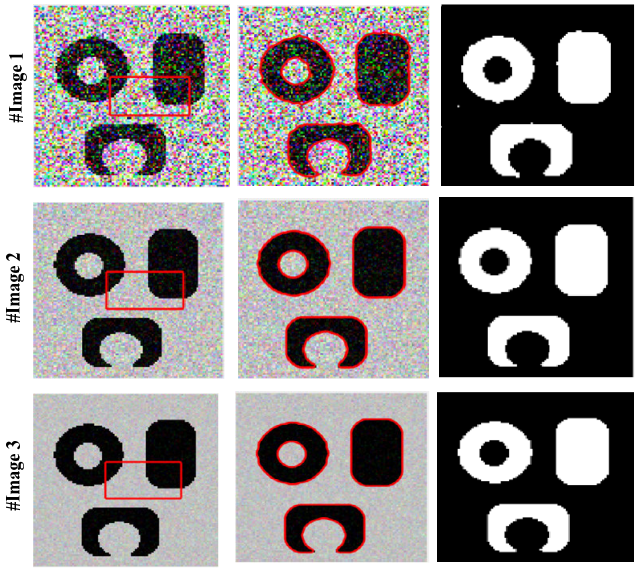

FIGURE 1. Segmentation results of the proposed model on synthetic image with different levels of Gaussian noise. Three rows of results correspond to Gaussian noise with mean 0 and sigma = 5, 10, and 15, respectively.

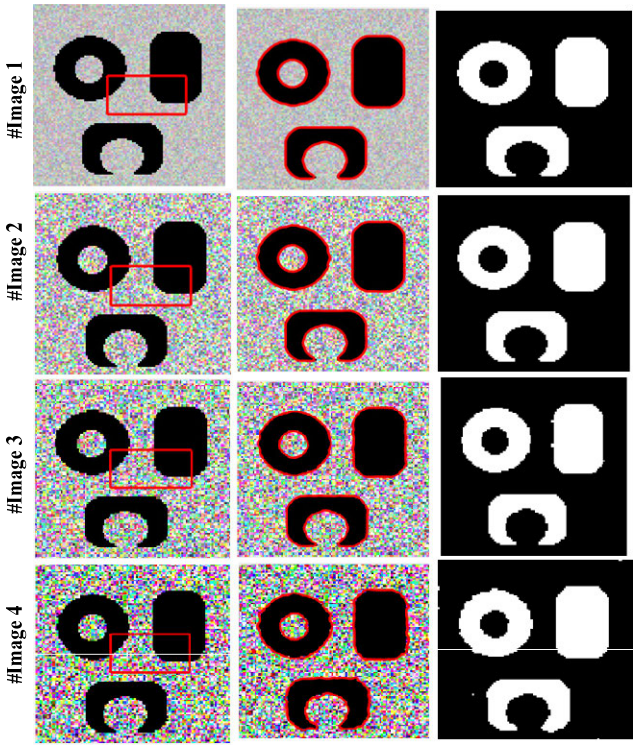

FIGURE 2. Segmentation results of the proposed model on synthetic image with different levels of speckle noise. Four rows of results correspond to speckle noise with mean 0 and variance 0.01, 0.1, 0.2, and 0.3, respectively.

A. EXPERIMENT RESULTS ON SYNTHETIC AND REAL IMAGES

To quantitatively validate the efficiency of the proposed model, we test synthetic images by adding different types of noise shown in Figs.1-3. In our experiments, the types of

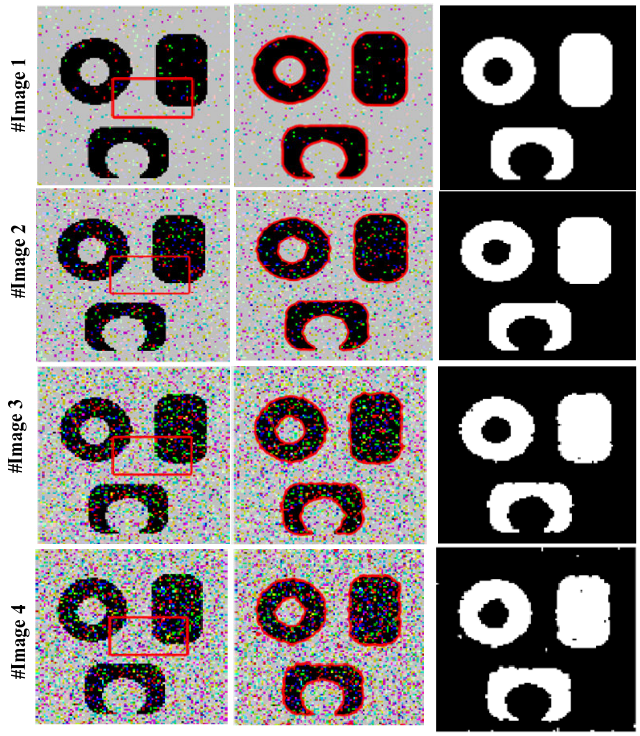

FIGURE 3. Segmentation results of the proposed model on synthetic image with different levels of salt and pepper noise. Four rows of results correspond to salt and pepper noise with densities of 0.05, 0.10, 0.15, and 0.20, respectively.

image noise consist of zero mean Gaussian noise, speckle noise, and salt and pepper noise. The parameters are set as follows: $\lambda_1 = \lambda_2 = 1$ and $\alpha = \beta = 0.5$. In Fig.1, three images in the 1st column are from the clean image corrupted by *Gaussian* noise with the mean 0 and sigma = 5, 10, and 15, respectively. In the 2nd column to the 3rd column, the final positions of the evolving curves and the segmentation results are shown, respectively. In Fig. 2, four images by adding different level speckle noises with mean 0 and variance 0.01, 0.1, 0.2, and 0.3 respectively, which is an inherent feature in ultrasound images, are shown in the 1st column. The final positions of the evolving curves and the segmentation results are shown in the 2nd column and the 3rd column, respectively. In Fig.3, the salt and pepper noise with densities of 0.05, 0.10, 0.15, and 0.20 respectively is fused into synthetic image shown in the 1st column. The final positions of the evolving curves and the segmentation results are shown in the 2nd column and the 3rd column, respectively. It can be seen that the proposed model can still extract three objects though the images is gravely corrupted by different types of noise.

Fig. 4 shows the segmentation results on natural images with different types of noise. The parameters in the experiment are set as follows: $\lambda_1 = \lambda_2 = 1$ and $\alpha = \beta = 0.5$. For color image, the average value of image intensity is written as $I = (I_R + I_G + I_B)/3$, where I_R, I_G and I_B denote the pixel values corresponding to the R, G, and

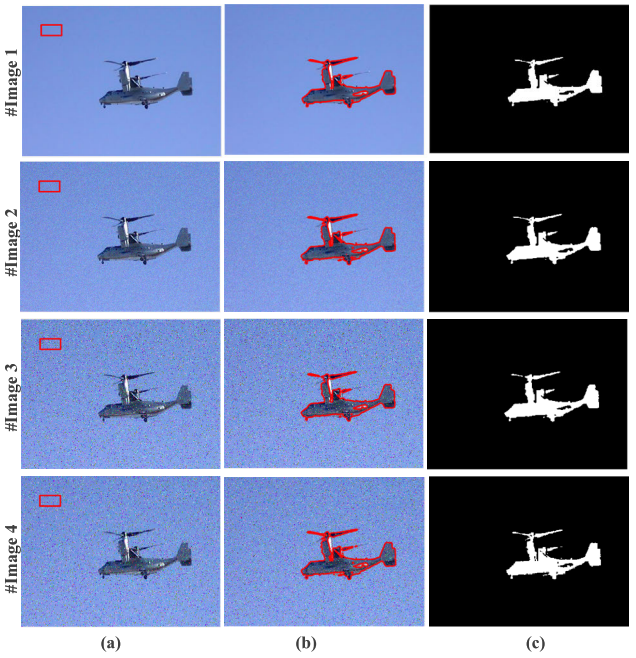

FIGURE 4. Segmentation results of the proposed model on natural image. The 1st column: The image with initial contour; The 2nd column: The final positions of the evolving curves; The 3rd column: The segmentation results of the proposed model.

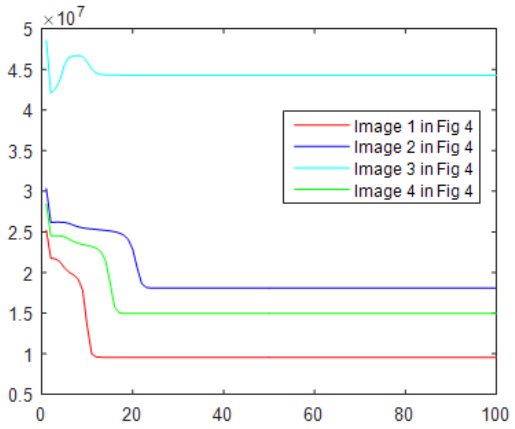

FIGURE 5. The total energy correspond to the images with different types of noise in Fig. 4 during 100 iterations.

B components, respectively. In the 1st column, the latter three images is generated by adding Gaussian noise with mean 0 and sigma = 15, speckle noise with mean 0 and variance 0.05, and salt and pepper noise with densities of 0.05, respectively. The final positions of the evolving curves are shown in the 2nd column and the 3rd column. The region energy during 100 iterations is shown in Fig. 5, respectively. According to the segmentation results, the proposed model is able to accurately extract desired objects and can rapidly converge to the global optima in less than 30 iterations. From these figures, it can be seen that the proposed model needs more iterations to reach steady state when the images contains more severe intensity inhomogeneity.

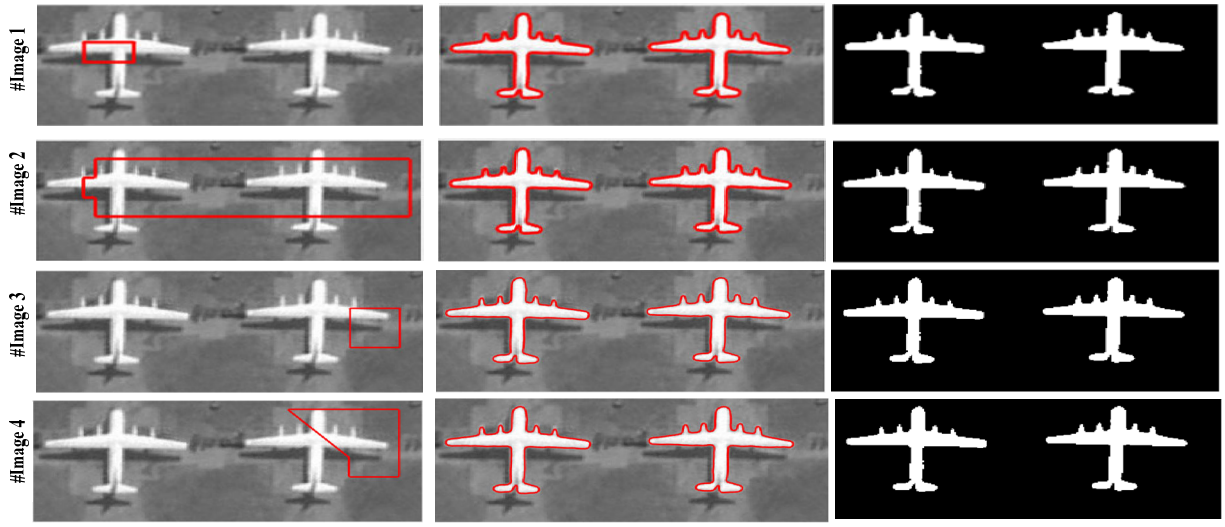

FIGURE 6. Segmentation results for natural image with different shapes. In the 1st column: Initial contours with different shapes; The 2nd column: The finial stopping positions; The 3rd column: The finial segmentation results.

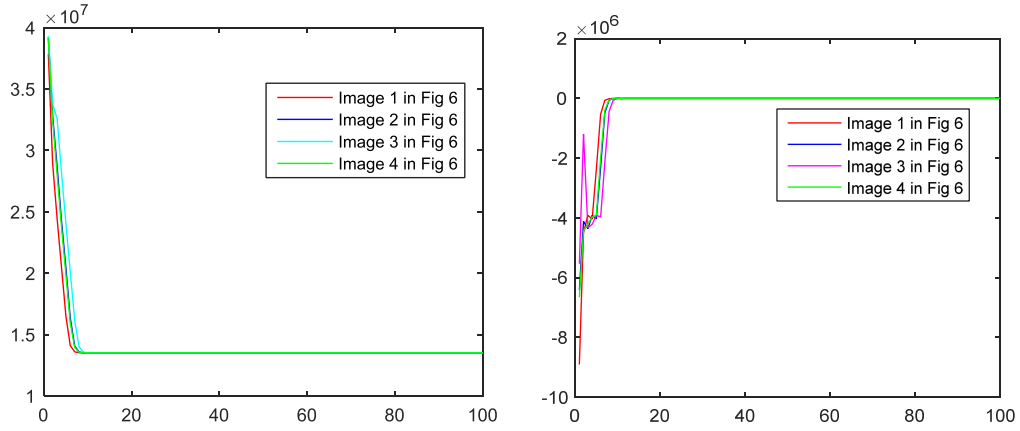

FIGURE 7. The final region energy and the changed energy corresponding to Fig. 6 during 100 iterations. (a) The final region energy during curve evolution; (b) The changed energy during curve evolution.

B. ROBUSTNESS TO INITIALIZATION

The following experiments is used to validate that the fuzziness of the energy can provide a balanced technique with a strong ability to reject local minima. Fig. 6 and Fig. 8 show the segmentation results of the proposed model with different initial shapes for images. The image in Fig. 8 is generated first corrupted by Gaussian noise with sigma = 10, followed by speckle noise with mean 0 and variance 0.1, and finally by salt and pepper noise with a density of 0.01. The parameters in the experiments are set as follows: $\lambda_1 = \lambda_2 = 1$ and $\alpha = \beta = 0.5$. In Fig. 6 and Fig. 8, different shapes with initial contour and the final stopping positions of the curves are shown in the 1st and 2nd columns, respectively, and the segmentation results are shown in the 3rd column. To clearly depict the running process of the proposed model, four fuzzy region energies corresponding to Fig. 6 and Fig. 8 are shown in Fig. 7(a) and Fig. 9(a) during 100 iterations, respectively. Fig. 7 (b) and Fig. 9 (b) show the difference between the new energy and old energy corresponding to Fig. 6 and Fig. 8, respectively. The segmentation results both show that the proposed model with different initial conditions (shapes and positions) can obtain similar results, the final stopping contours are almost the same, and the proposed model reaches the steady state in less than 10 iterations. In conclusion, our model is robust to initialization.

C. COMPARISION WITHTHE POPULAR REGION-BASED ACMS

To demonstrate the performance of the proposed model, we compare the proposed model with the popular region-based ACMs, such as the Chan-Vese model [6], the LBF model [9], the LIF model [12], the FEBAC model [24], the GL-FEBAC model [25], and FEACC [26]. The codes of the LIF model is available at http://www.kaihuazhang.net/.

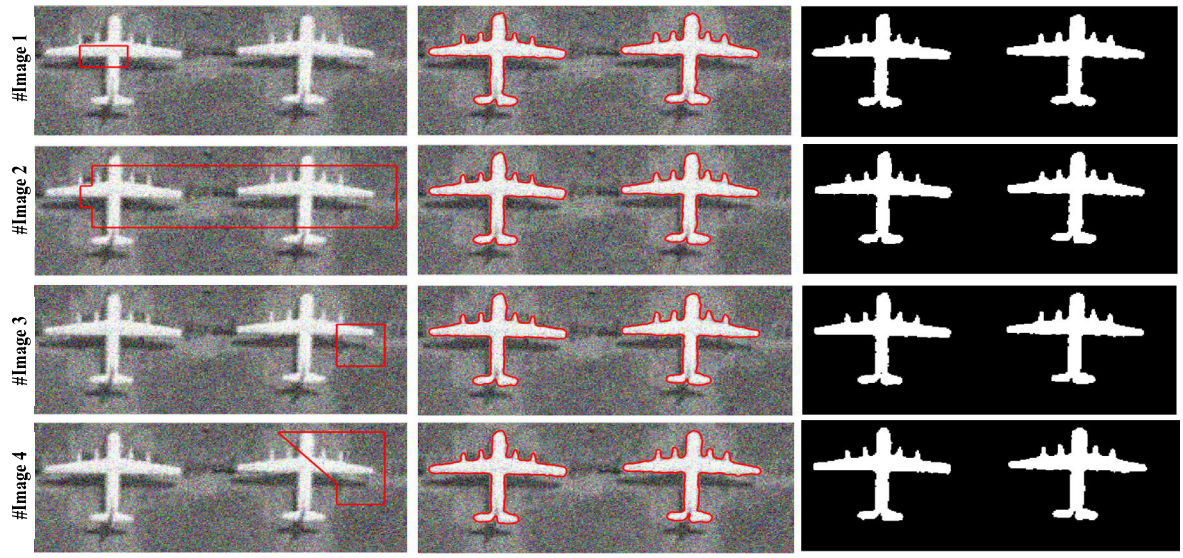

FIGURE 8. Segmentation results for natural image by adding hybrid noise with different shapes. In the 1st column: Initial contours with different shapes; The 2nd column: The finial stopping positions; The 3rd column: The finial segmentation results.

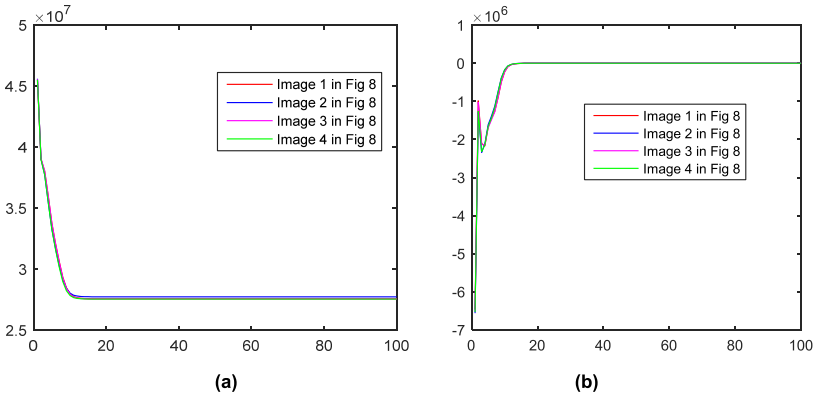

FIGURE 9. The final region energy and the changed energy corresponding to Fig. 8 during 100 iterations. (a) The final region energy during curve evolution; (b) The changed energy during curve evolution.

To quantitatively evaluate these region-based ACMs, we use Dice coefficient [30] to measure performance with ground truth and region entropy [31] to measure performance without ground truth. Dice coefficient between two regions P and Q is defined as follows:

$$J(P, Q) = \frac{2 \times |P \cap Q|}{|P| + |Q|} \tag{25}$$

where $|P|$, $|Q|$ and $|P \cap Q|$ are the pixel number of two regions P, Q, and their union area, respectively. The closer the value $J(P, Q)$ is to 1, the better the segmentation results is.

The region entropy is defined as:

$$RE = E_l(I) + E_r(I) \tag{26}$$

where $E_l(I)$ and $E_r(I)$ are a layout entropy and an desired region entropy, respectively.

Here, $E_l(I)$ and $E_r(I)$ are defined as follows:

$$E_l(I) = -\sum_{i=1}^{N} \left(\frac{S_i}{S_I}\right) \log\left(\frac{S_i}{S_I}\right) \tag{27}$$

$$E_r(I) = -\sum_{i=1}^{N} \left(\frac{S_i}{S_I}\right) \sum\nolimits_m \left(\frac{L_i(m)}{S_i}\right) \log\left(\frac{L_i(m)}{S_i}\right) \tag{28}$$

where S_i/S_I is the probability of a pixel belong to region R_i, and $L_i(m)$ is the number of pixels in region R_i which has value m of a luminance.

To validate the robustness of the proposed model, the segmented images from MSRA-B database are firstly corrupted by Gaussian noise with sigma = 15, followed by speckle noise with mean 0 and variance 0.05, and finally by salt and pepper noise with a density of 0.05. Figs. 10-11 depict the segmentation results of natural images using different region-based ACMs. Since the images includes severe intensity

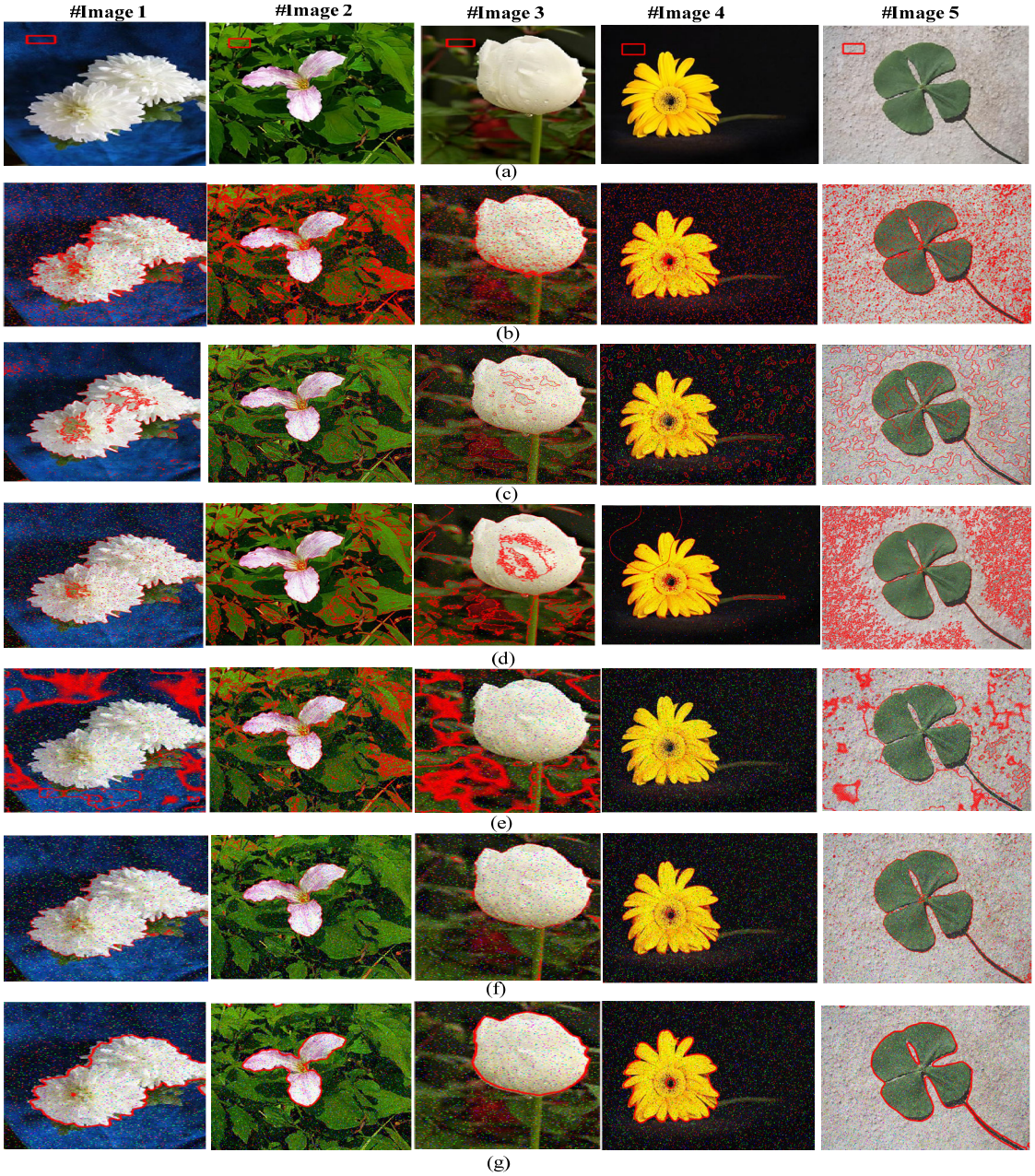

FIGURE 10. The final stopping positions for natural image from MSRA-B database using different models. (a) The original image with initial curves; (b) C-V; (c) LIF; (d) LBF; (e) FEBAC; (f) GL-FEBAC; (g) the proposed model.

inhomogeneity, accurately extracting the desired object boundaries of these images is a challenging task. From Figs.10-11, it can be seen only the proposed model can exactly extract the objects in five images, and the Chan-Vese model extract the brightest regions, while the GL-FEAC models can obtain better results than other ACMs (LIF, LBF and FEAC). To clearly present the performance and efficiency, comparative results in terms of Dice coefficient and average running time are shown in Tables 1-2. From these tables, it is also seen that the Chan-Vese model and the LIF model occupied the most running time of all the segmented images because these models with convolutional operation need more running time. On the other hand, the FEAC model takes the least average time while our model takes minimum executing time. The models based fuzzy energy-base active

TABLE 1. Comparison of the popular ACMs in terms of Dice coefficient.

Image	C-V	LBF	LIF	FEAC	GL-FEAC	Our
Image 1	0.8352	0.5941	0.8014	0.4128	0.9004	**0.9732**
Image 2	0.7546	0.5107	0.5821	0.9014	0.8848	**0.9684**
Image 3	0.7845	0.4864	0.5148	0.3876	0.8462	**0.9548**
Image 4	0.7364	0.5149	0.4736	0.5973	0.9014	**0.9476**
Image 5	0.7018	0.5218	0.4428	0.6873	0.8764	**0.9747**

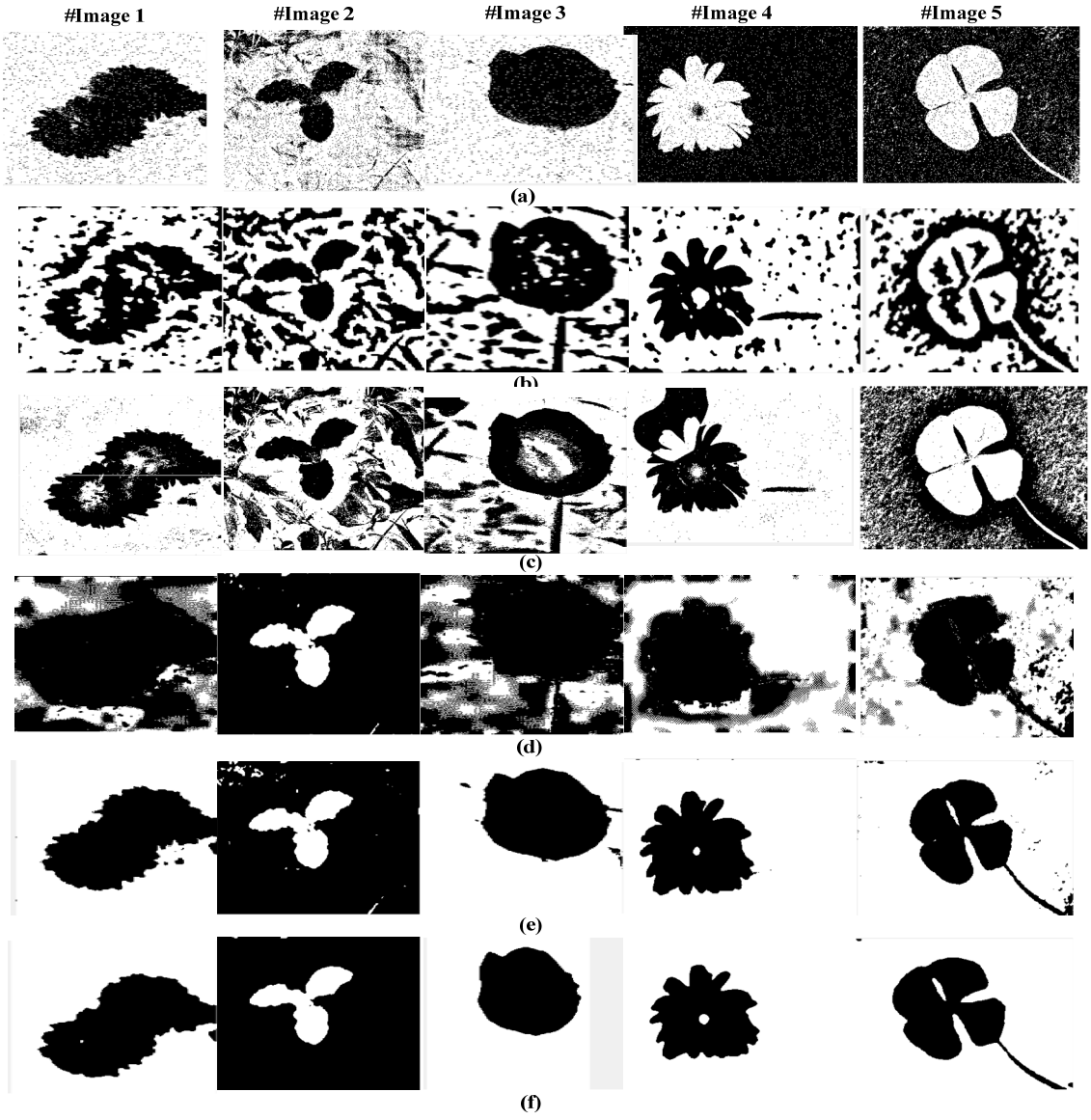

FIGURE 11. Segmentation results in Fig. 10 using different models. (a) C-V; (b) LIF; (c) LBF; (d) FEBAC; (e) GL-FEBAC; and (f) the proposed model.

TABLE 2. Comparison of the region-based ACMs in terms of running time(Seconds).

Method	IterNum	Time	Time	Time	Time	Time
C-V	500	88.156	101.25	79.471	79.254	94.483
LBF	220	33.039	50.428	30.255	38.757	40.278
LIF	450	106.261	130.327	93.553	96.036	114.601
FEAC	100	50.4947	43.438	57.897	43.554	60.418
GL-FEAC	100	62.754	52.4668	62.181	55.575	71.598
Our	100	**2.912**	**3.014**	**2.911**	**2.832**	**3.176**

TABLE 3. Comparison of the region-based ACMs in terms of region entropy.

Image	Chan-Vese	LBF	LIF	FEAC	GL-FEAC	Our
Image 1	4.849	5.024	5.526	4.849	4.762	**4.215**
Image 2	4.688	4.723	4.753	5.286	5.152	**4.308**
Image 3	5.114	5.476	5.582	5.790	4.876	**4.243**
Image 4	4.624	6.247	6.336	5.548	5.643	**4.279**

contour have fast convergence due to its strictly convex energy.

To further validate robustness of the proposed model, cell images with severe intensity inhomogeneity are tested shown in Figs. 12-13. In Fig. 12, to enhance intensity inhomogeneity in given images, the 2^{nd}, 3^{rd} and 4^{th} cell images are first corrupted by Gaussian noise with sigma = 15, followed by speckle noise with mean 0 and variance 0.05, and finally by salt and pepper noise with a density of 0.05. From Figs. 12-13, we obverse that only the proposed model

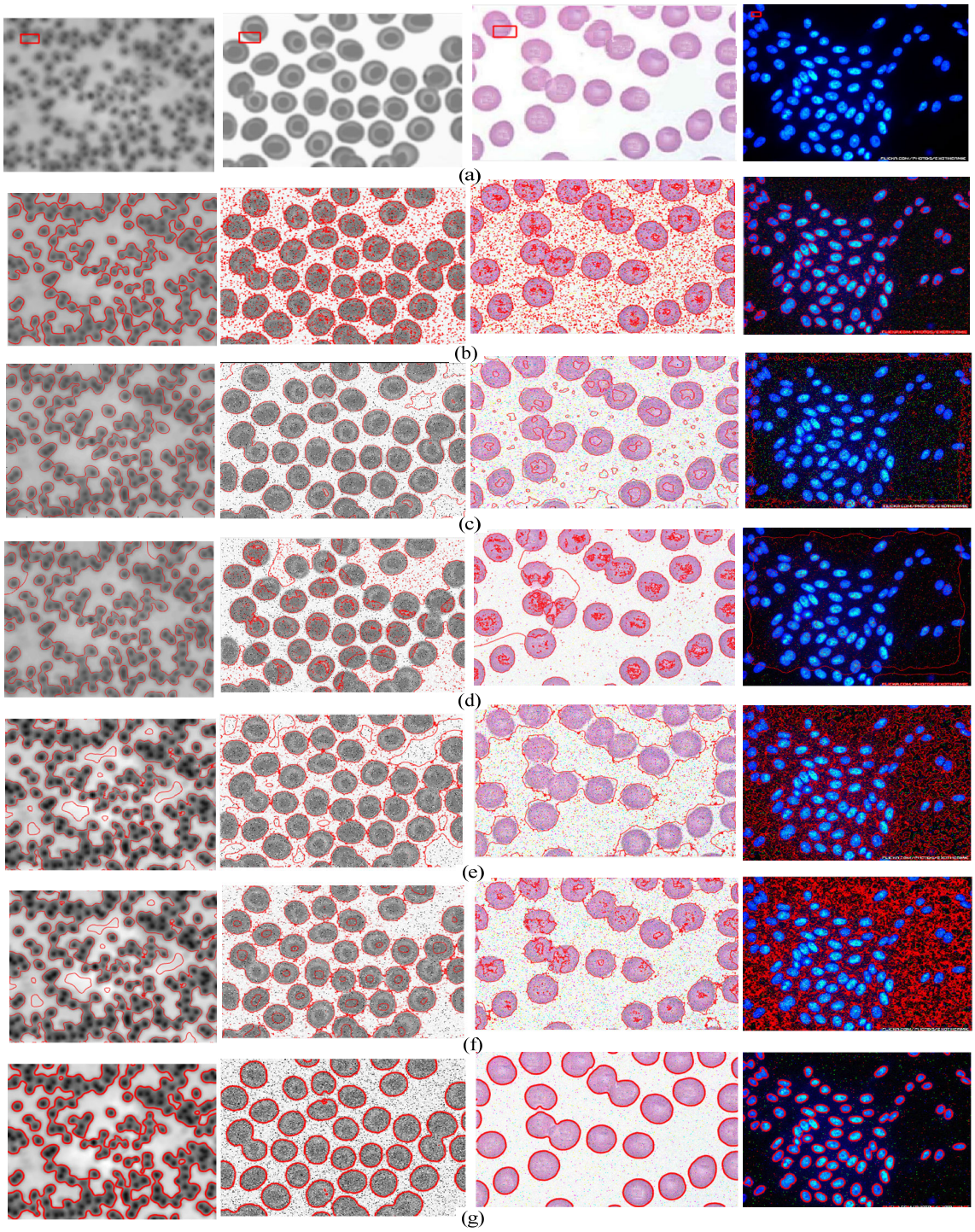

FIGURE 12. The final stopping positions for natural image using different models. (a) The original image with initial curve; (b) C-V; (c) LIF; (d) LBF; (e) FEBAC; (f) GL-FEBAC; (g) the proposed model.

can exactly extract the objects in four cell images with severe intensity inhomogeneity. The corresponding comparative results in terms of region entropy and average running time are shown in Tables 3-4. From these tables, it is also seen that the proposed model has the largest values in terms of average Dice coefficient in all of the region-based ACMs. Moreover, since our method update the pseudo LSF of the entire image domain for each iteration, the proposed model takes the least running time. In addition, the convex fuzzy region energy causes fast convergence.

In Fig.14, we select a complex medical image to further validate our proposed model. The input image with initial

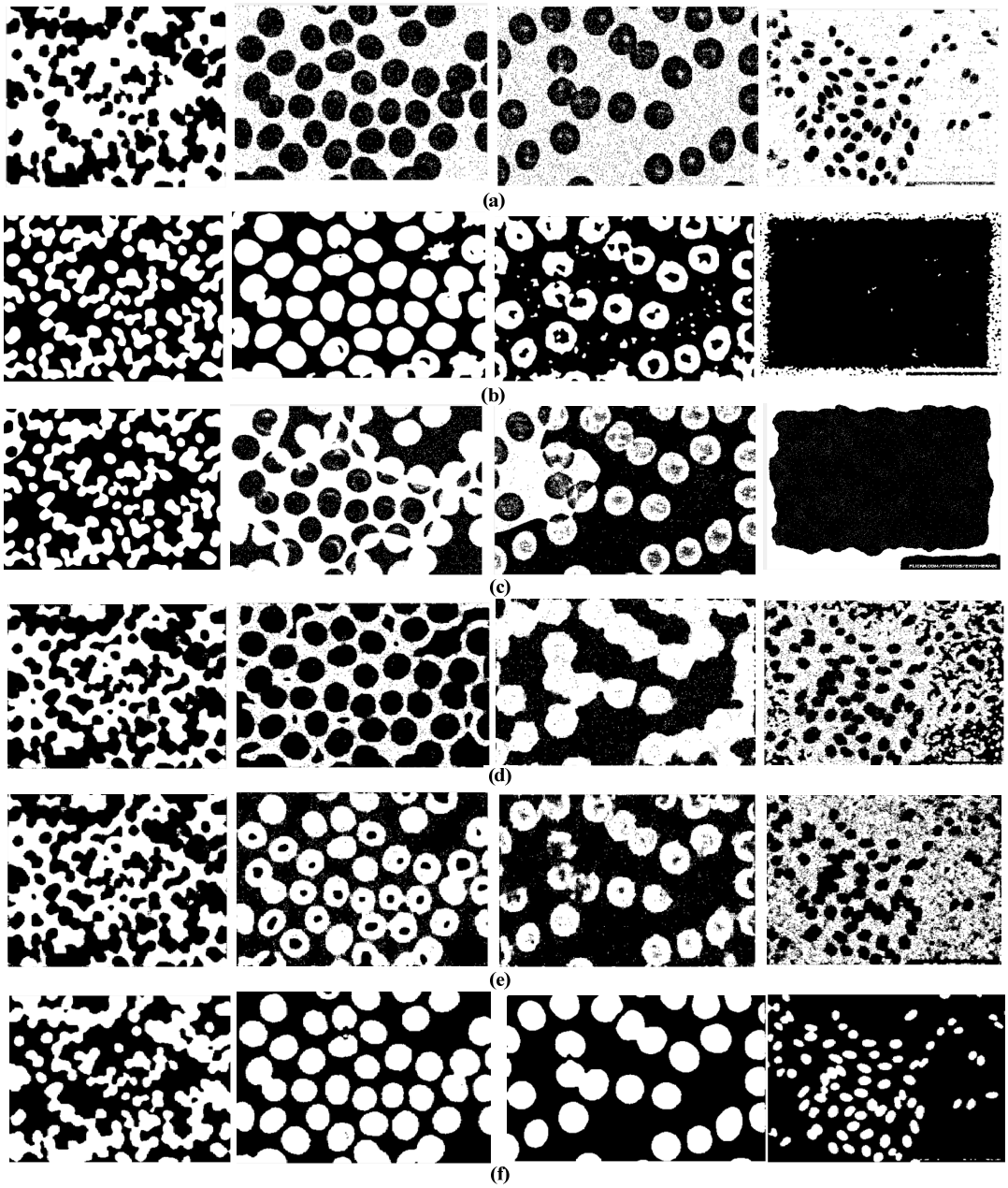

FIGURE 13. Segmentation results corresponding to Fig. 12 using different models. (a) C-V; (b) LIF; (c) LBF; (d) FEAC; (e) GL-FEAC; and (f) the proposed model.

TABLE 4. Comparison of the region-based ACMs in terms of running time and iterations.

Segmentation model	Image 1		Image 2		Image 3		Image 4	
	Time	Iterations	Time	Iterations	Time	Iterations	Time	Iterations
C-V	13.328	240	13.058	160	13.111	180	21.466	200
LBF	81.803	220	52.653	220	51.516	220	208.291	220
LIF	142.851	450	141.219	450	96.036	450	583.405	450
FEAC	60.4366	100	64.316	100	58.201	100	427.049	100
GL-FEAC	71.335	100	73.4668	100	69.932	100	479.896	100
Our	**3.949**	**40**	**4.437**	**40**	**8.648**	**40**	**14.854**	**40**

curve is shown in Fig. 14(a). The segmentation results using the C-V model, LIF model, FEACC model, and the proposed model are shown in Fig. 14(b)-(e), respectively. From Fig. 14, the C-V model includes more noise than other models because it is based on the global image information. However, the FEACC loses detailed information due to its local

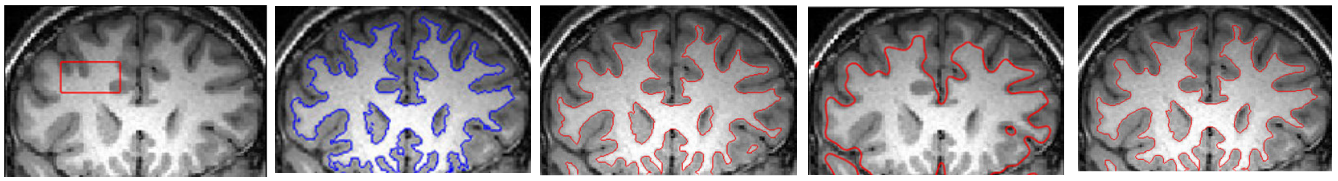

FIGURE 14. Segmentation results using different models. (b) Input image with initial curve; (b) C-V; (c) LIF; (d) FEACC; (e) Our model.

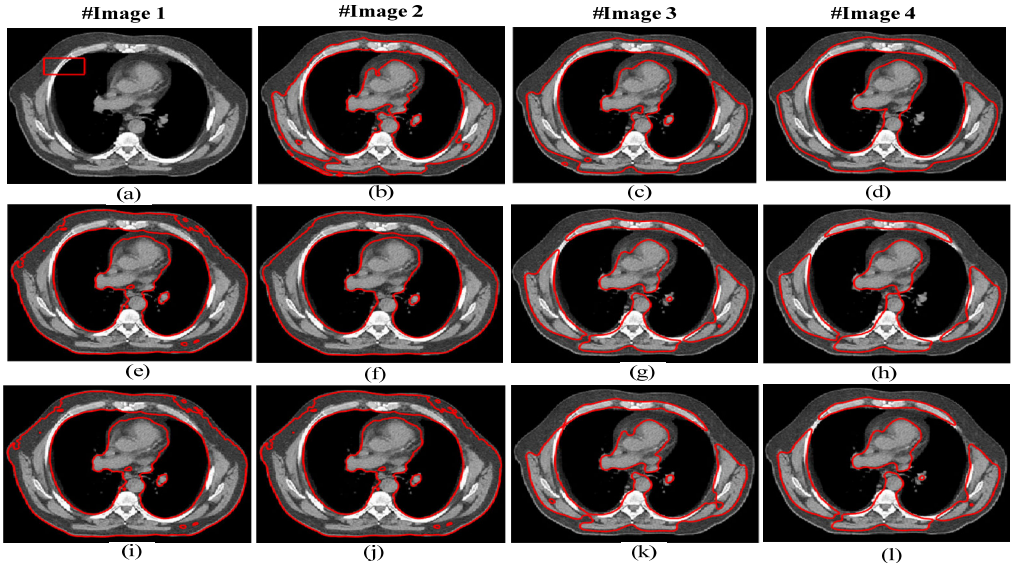

FIGURE 15. The segmentation results of the proposed model with different parameters for medical image. (a) The original image with initial contour; (b-d) Keeping $\alpha = \beta = 0.5$ and the windows size $k = 3$ fixed, the parameters λ_1 and λ_2 are set to $(0.1, 0.9)$, $(0.5, 0.5)$, and $(0.9, 0.1)$, respectively; (e-h) Keeping $\lambda_1 = \lambda_2$ and $\alpha = \beta = 0.5$ fixed, the windows size k is set at 9, 7, 5 and 3; (i-l) Keeping $\lambda_1 = \lambda_2$ and the windows size $k = 5$ fixed, the weighting parameters α and β are set at $(1, 0)$, $(0.9, 0.1)$, $(0.5, 0.5)$ and $(0.1, 0.9)$, respectively.

spatial information. Among these models, our proposed model can obtain similar results with the LIF model. But the LIF model is sensitive to initial position.

D. EFFECT OF PARAMETERS

The parameters play an important role in segmenting the object(s). In our model, there are three important parameters to decide the segmentation performance: the weights α and β, and the radius of the local windows k. The radius of the local window is used to decide the degree of intensity inhomogeneity and smooth the pseudo LSF. In general, more severer intensity inhomogeneity and more noise the segmented image includes, a larger value of the size of a local window is selected. The weights α and β of the approximated images is to control the degree of intensity inhomogeneity in given image. If the image contains severe intensity inhomogeneity, a large value α should be chosen, and vice versa.

To illustrate the effect of parameters, the segmentation results with different parameters on medical images with severe intensity inhomogeneity are shown in Fig.15. The image with initial curve is shown in Fig. 15(a). In Fig. 15(b)-(d), we keep $\alpha = \beta = 0.5$ and the radius of the local window $k = 5$ fixed, and set weighting parameters λ_1 and λ_2 to $(0.1, 0.9)$, $(0.5, 0.5)$, and $(0.9, 0.1)$, respectively. Then, in Fig. 15(e)-(h), we keep the parameters $\lambda_1 = \lambda_2 = 1$ and $\alpha = \beta = 0.5$ fixed, and change the radius of the local windows to 9, 7, 5 and 3. Finally, in Fig. 15(i)-(l), the parameters $\lambda_1 = \lambda_2 = 1$ and the radius of the local windows $k = 5$ fixed, the weighting parameters α and β are set at $(0, 1)$, $(0.1, 0.9)$, $(0.5, 0.5)$ and $(0.9, 0.1)$, respectively. From these results, it can be seen that the constants λ_1 and λ_2 have little influence on the proposed model. In our experiment, the constants $\lambda_1 = \lambda_2 = 1$ are to balance the object and background region. The larger the weight value α is, the higher intensity inhomogeneity the proposed model can handle, and vice versa. With the decrease of the radius of the local windows shown in Fig. 15 (e)-(h), the ability of the proposed model to extract local image information is weaken. But too large value may lead to too many small objects to extract, so a reasonable radius of the local windows is selected in terms of the degree of intensity inhomogeneity.

V. CONCLUSION

In this paper, we present a fuzzy region-based active contour model driven by weighting global and local fitting energy to segment the images with intensity inhomogeneity. The proposed model includes two parts: fuzzy region energy and edge energy. In the first part, the fuzzy region energy, which has been proved to be strictly convex, is formulated with local

spatial image information and is used to drive the motion of the evolving curve(s). In the second part, an edge energy is designed in order to make the evolving curve accurately stop the object boundaries. Instead of using the Euler-Lagrange equation to minimize the fuzzy region energy, a direct method by computing the difference between the old and new energy functions is developed to update the pseudo LSF in the whole image domain for each iteration. The experimental results show that the proposed model can successfully extract the object from both synthetic and real images with noise and intensity inhomogeneity. But our method cannot segment the images when the object is very similar to the background region. In future, our model can be applied to many famous ACMs, such as kernel space [33] and multi-phase image segmentation [12].

APPENDIX A

The fuzzy energy function in (16) can be written as follows:

$$F^{fr}(u) = \lambda_1 F_A^{fr}(u, g) + \lambda_2 F_B^{fr}(u, g), \quad u \in [0, 1] \tag{A-1}$$

where $F_A^{fr}(u, g)$ and $E_B^{fr}(u, g)$ are defined as:

$$F_A^{fr}(u, g) = \int_\Omega [u(x)]^m \, g \, (I(x) - (\alpha f_o + \beta c_1))^2 \, dx \tag{A-2}$$

$$F_B^{fr}(u, g) = \int_\Omega [1 - u(x)]^m \, g \, (I(x) - (\alpha f_b + \beta c_2))^2 \, dx \tag{A-3}$$

The equation $F_A^{fr}(u, g)$ in (A-2) can be written as

$$\varepsilon_A^{fr}(x, g) = [u(x)]^m \, g \, (I(x) - (\alpha f_o + \beta c_1))^2 \tag{A-4}$$

and $F_A^{fr}(u, g) = \int_\Omega \varepsilon_A^{fr}(x, g)dx$.

Now we first prove the equation $\varepsilon_A^{fr}(x, g)$ is convex. Let $x_1, x_2 \in \Omega$, for $\forall\theta \in [0, 1]$.Then we have

$$\theta x_1 + (1 - \theta)x_2 = \theta(x_1 - x_2) + x_2 \in \Omega \tag{A-5}$$

Therefore, the domain of $\varepsilon_A^{fr}(x, g)$ is convex. The second order derivative of (A-4) w. r. t. u, and we have

$$\frac{\partial^2 \varepsilon_A^{fr}}{\partial u^2} = \frac{\partial}{\partial u}\left(\frac{\partial \varepsilon_A^{fr}}{\partial u}\right) = \frac{\partial}{\partial u}\left(m\,[u(x)]^{m-1} \, g \, (I(x) - (\alpha f_o + \beta c_1))^2\right)$$
$$= m(m-1)\,[u(x)]^{m-2} \, g \, (I(x) - (\alpha f_o + \beta c_1))^2 \tag{A-6}$$

Since $m > 1$, $u(x) \in [0, 1]$, and $g \, (I(x) - (\alpha f_o + \beta c_1))^2 \geq 0$, so $\partial^2 \varepsilon_A^{fr} / \partial u^2 \geq 0$.

Since the domain of $\varepsilon_A^{fr}(x, g)$ is convex and $\partial^2 \varepsilon_A^{fr} / \partial u^2 \geq 0$, so $\varepsilon_A^{fr}(x, g)$ is convex. Therefore, $\forall x_1, x_2 \in \Omega$ and $\theta \in [0, 1]$, and we can get the following relation:

$$\varepsilon_A^{fr}(\theta x_1 + (1 - \theta)x_2) \leq \theta \varepsilon_A^{fr}(x_1) + (1 - \theta)\varepsilon_A^{fr}(x_2) \tag{A-7}$$

Calculating the integral of the two sides of (A-7), we can obtain the following formulation:

$$\int_\Omega \varepsilon_A^{fr}(\theta x_1 + (1 - \theta)x_2)dx \leq \theta \int_\Omega \varepsilon_A^{fr}(x_1)dx + (1 - \theta) \int_\Omega \varepsilon_A^{fr}(x_2)dx \tag{A-8}$$

With $F_A^{fr}(u, g) = \int_\Omega \varepsilon_A^{fr}(x, g)dx$, (A-8) can be rewritten as:

$$F_A^{fr}(\theta x_1 + (1 - \theta)x_2) \leq \theta F_A^{fr}(x_1) + (1 - \theta)F_A^{fr}(x_2) \tag{A-9}$$

Hence, F_A^{fr} is convex.
Similarly, let

$$\varepsilon_B^{fr}(x) = [1 - u(x)]^m \, g \, (I(x) - (\alpha f_b + \beta c_2))^2 \tag{A-10}$$

where $\varepsilon_B^{fr} : \Omega \to R$. The equation (A-2) is written as $F_B^{fr}(u, g) = \int_\Omega \varepsilon_B^{fr}(x, g)dx$. In the same way, we can also prove that the formulas $F_B^{fr}(u, g)$ is convex.

In (A-1), since $\lambda_1 > 0$ and $\lambda_2 > 0$, then the region energy $F^{fr}(u)$ consists of two weighting convex functionals. So the energy function $F^{fr}(u)$ is convex with regard to u.

APPENDIX B

Two constants $\boldsymbol{c}_1$ and $\boldsymbol{c}_2$ in (7) are converted into discrete space and written as:

$$c_1 = \frac{\sum_\Omega I(x) \cdot [u(x)]^m}{\sum_\Omega [u(x)]^m} c_2 = \frac{\sum_\Omega I(x) \cdot [1 - u(x)]^m}{\sum_\Omega [1 - u(x)]^m} \tag{B-1}$$

where $u(x)$ is the degree of membership for pixel x, and $I(x)$ is the corresponding intensity value.

Two local average intensities f_o and f_b in (13) with weighting function $\omega(x, y)$ are expressed as:

$$f_o = \frac{\sum_\Omega \omega(x, y) * [I(x)[u(x)]^m]}{\sum_\Omega \omega(x, y) * [u(x)]^m} \tag{B-2}$$

$$f_b = \frac{\sum_\Omega \omega(x, y) * [I(x)[1 - u(x)]^m]}{\sum_\Omega \omega(x, y) * [1 - u(x)]^m} \tag{B-3}$$

For point P, suppose that the degree of membership is u_0, the intensity value is I_0. When the new degree of membership is changed into u_n, the constants c_1, c_2, f_o and f_b correspondingly become new constants $\hat{c}_1$, $\hat{c}_2$, $\hat{f}_o$ and $\hat{f}_b$. The new constant $\hat{c}_1$ is computed as follows:

$$\hat{c}_1 = \frac{\sum_\Omega I(x) \cdot \left[\hat{u}(x)\right]^m}{\sum_\Omega \left[\hat{u}(x)\right]^m} = \frac{\sum_\Omega I(x) \cdot [u(x)]^m + (u_n^m I_0 - u_0^m I_0)}{\sum_\Omega [u(x)]^m + (u_n^m - u_0^m)}$$
$$= \frac{t_1 c_1 + I_0(u_n^m - u_0^m)}{t_1 + (u_n^m - u_0^m)} = c_1 + \frac{\Delta u_1}{t_1 + \Delta u_1}(I_0 - c_1) \tag{B-4}$$

where $t_1 = \sum_\Omega [u(x)]^m$, and $\Delta u_1 = u_n^m - u_0^m$. In the same way, we can obtain the new values $\hat{c}_2$

$$\hat{c}_2 = c_2 + \frac{\Delta u_2}{t_2 + \Delta u_2}(I_0 - c_2) \tag{B-5}$$

where $t_2 = \sum_\Omega [1 - u(x)]^m$ and $\Delta u_2 = (1 - u_n)^m - (1 - u_0)^m$.

The new pixel average intensities $\hat{f}_o$ are expressed as follows:

$$\hat{f}_o = \frac{\sum_\Omega \omega(x, y) * \left[I(x)[\hat{u}(x)]^m\right]}{\sum_\Omega [\hat{u}(x)]^m * \omega(x, y)}$$
$$= \frac{\sum_\Omega \omega(x, y) * \left(I(x)[u(x)]^m + u_n^m I_0 - u_0^m I_0\right)}{\sum_\Omega \omega(x, y) * \left([u(x)]^m + u_n^m - u_0^m\right)}$$
$$= \frac{\sum_\Omega \omega(x, y) * I(x)[u(x)]^m + \omega(x, y) * \Delta u_1 I_0}{\sum_\Omega \omega(x, y) * [u(x)]^m + \omega(x, y) * \Delta u_1} \tag{B-6}$$

where $*$ is convolution operation. From (B-2), we can get:

$$\sum_{\Omega} \omega(x,y) * \left[I(x)[u(x)]^m\right] = f_o \omega(x,y) * \sum_{\Omega} [u(x)]^m = f_o \omega(x,y) * t_1 \quad \text{(B-7)}$$

Combing (B-6) and (B-7), we can get:

$$\begin{aligned}\hat{f}_o &= \frac{\sum_{\Omega} \omega(x) * I(x)[u(x)]^m + \omega(x,y) * \Delta u_1 I_0}{\sum_{\Omega} \omega(x,y) * [u(x)]^m + \omega(x,y) * \Delta u_1} \\ &= \frac{f_o \omega(x,y) * t_1 + I_0 \omega(x,y) * \Delta u_1}{\omega(x,y) * t_1 + \omega(x,y) * \Delta u_1} \\ &= f_o + \frac{I_0 \omega(x,y) * \Delta u_1 - f_o \omega(x,y) * \Delta u_1}{\omega(x,y) * t_1 + \omega(x,y) * \Delta u_1} \\ &= f_o + \frac{(I_0 - f_o)\, \omega(x,y) * \Delta u_1}{\omega(x,y) * t_1 + \omega(x,y) * \Delta u_1} \end{aligned} \quad \text{(B-8)}$$

In the same way, we can also obtain the new $\hat{f}_b$:

$$\hat{f}_b = f_b + \frac{(I_0 - f_b)\, \omega(x,y) * \Delta u_2}{\omega(x,y) * t_2 + \omega(x,y) * \Delta u_2} \quad \text{(B-9)}$$

It is easy to calculate the change of the fuzzy region energy using the formulations defined in (B-2)-(B-5). For the same point P, when the degree of membership is changed from u_0 into u_n, the fuzzy region energy F^{fr} is correspondingly changed into $\hat{F}^{fr}$. First, we give the energy F^{fr} in (16) in the discrete space as follows:

$$\begin{aligned} F^{fr} &= F_A^{fr} + F_B^{fr} = \lambda_1 \sum_{\Omega} [u(x)]^m\, g\, (I(x) - (\alpha f_o + \beta c_1))^2 \\ &\quad + \lambda_2 \sum_{\Omega} [1 - u(x)]^m\, g\, ((I(x) - (\alpha f_b + \beta c_2))^2 \end{aligned} \quad \text{(B-10)}$$

with

$$F_A^{fr} = \lambda_1 \sum_{\Omega} [u(x)]^m\, g\, (I(x) - (\alpha f_o + \beta c_1))^2 \quad \text{(B-11)}$$

$$F_B^{fr} = \lambda_2 \sum_{\Omega} [1 - u(x)]^m\, g\, ((I(x) - (\alpha f_b + \beta c_2))^2 \quad \text{(B-12)}$$

Correspondingly, the new energy $\hat{F}^{fr}$ is represented as:

$$\begin{aligned} \hat{F}^{fr} = \hat{F}_A^{fr} + \hat{F}_B^{fr} &= \lambda_1 \sum_{\Omega} \left[\hat{u}(x)\right]^m g \left(I(x) - \left(\alpha \hat{f}_o + \beta \hat{c}_1\right)\right)^2 \\ &\quad + \lambda_2 \sum_{\Omega} \left[1 - \hat{u}(x)\right]^m g \left(I(x) - (\alpha \hat{f}_b + \beta \hat{c}_2)\right)^2 \end{aligned} \quad \text{(B-13)}$$

with

$$\hat{F}_A^{fr} = \lambda_1 \sum_{\Omega} \left[\hat{u}(x)\right]^m g \left(I(x) - \left(\alpha \hat{f}_o + \beta \hat{c}_1\right)\right)^2 \quad \text{(B-14)}$$

$$\hat{F}_B^{fr} = \lambda_2 \sum_{\Omega} \left[1 - \hat{u}(x)\right]^m g \left(I(x) - (\alpha \hat{f}_b + \beta \hat{c}_2)\right)^2 \quad \text{(B-15)}$$

In the following, we separately compute the new formulas $\hat{F}_A^{fr}$ and $\hat{F}_B^{fr}$. The new formula $\hat{F}_A^{fr}$ is computed as:

$$\begin{aligned} \hat{F}_A^{fr} &= \sum_{\Omega} \left[\hat{u}(x)\right]^m g \left(I(x) - \left(\alpha \hat{f} + \beta \hat{c}_1\right)\right)^2 \\ &= \sum_{\Omega} [u(x)]^m g \left(I(x) - \left(\alpha \hat{f}_o + \beta \hat{c}_1\right)\right)^2 \\ &\quad + g \left(u_n^m - u_0^m\right) \left(I_0 - \left(\alpha \hat{f}_o + \beta \hat{c}_1\right)\right)^2 \end{aligned} \quad \text{(B-16)}$$

To simplify the above equation, we first calculate the equations $(I(x) - (\alpha \hat{f}_o + \beta \hat{c}_1))^2$ and $(I_0 - (\alpha \hat{f}_o + \beta \hat{c}_1))^2$ by inserting (B-4) and (B-8), then

$$\begin{aligned} &\left(I(x) - \left(\alpha \hat{f}_o + \beta \hat{c}_1\right)\right)^2 \\ &= (I(x) - (\alpha (f_o + \frac{\omega(x,y) * \Delta u_1\, (I_0 - f_o)}{\omega(x,y) * (t_1 + \Delta u_1)} \\ &\quad + \beta (c_1 + \frac{\Delta u_1}{t_1 + \Delta u_1} (I_0 - c_1)))^2 \\ &= \left(I(x) - (\alpha f_o + \beta c_1) - \left(\alpha \frac{\omega(x,y) * \Delta u_1\, (I_0 - f_o)}{\omega(x,y) * t_1 + \omega(x,y) * \Delta u_1} \right.\right. \\ &\quad \left.\left. + \ \beta \frac{\Delta u_1}{t_1 + \Delta u_1} (I_0 - c_1)\right)\right)^2 \\ &= \left(\alpha \frac{\omega(x,y) * \Delta u_1\, (I_0 - f_o)}{\omega(x,y) * t_1 + \omega(x,y) * \Delta u_1} + \beta \frac{\Delta u_1}{t_1 + \Delta u_1} (I_0 - c_1)\right)^2 \\ &\quad + (I(x) - (\alpha f_o + \beta c_1))^2 - 2\, (I(x) - (\alpha f_o + \beta c_1)) \\ &\quad \left(\alpha \frac{\omega(x,y) * \Delta u_1\, (I_0 - f_o)}{\omega(x,y) * t_1 + \omega(x,y) * \Delta u_1} + \beta \frac{\Delta u_1}{t_1 + \Delta u_1} (I_0 - c_1)\right) \end{aligned} \quad \text{(B-17)}$$

$$\begin{aligned} &\left(I_0 - (\alpha \hat{f}_o + \beta \hat{c}_1)\right)^2 = (I_0 - (\alpha f_o + \beta c_1) \\ &\quad - (\alpha \frac{\omega(x,y) * \Delta u_1\, (I_0 - f_o)}{s_1 + \omega(x,y) * \Delta u_1} + \beta \frac{\Delta u_1}{t_1 + \Delta u_1} (I_0 - c_1)))^2 \\ &= (\alpha\, (I_0 - f_o) + \beta\, (I_0 - c_1) \\ &\quad - (\alpha \frac{\omega(x,y) * \Delta u_1\, (I_0 - f_o)}{\omega(x,y) * t_1 + \omega(x,y) * \Delta u_1} + \beta \frac{\Delta u_1}{t_1 + \Delta u_1} (I_0 - c_1)))^2 \\ &= \left(\frac{\alpha \omega(x,y) * t_1\, (I_0 - f_o)}{\omega(x,y) * (t_1 + \Delta u_1)} + \frac{\beta t_1 (I_0 - c_1)}{t_1 + \Delta u_1}\right)^2 \end{aligned} \quad \text{(B-18)}$$

Combing (B-16), (B-17) and (B-18), the formulation $\hat{F}_A^{fr}$ can be written as:

$$\begin{aligned} \hat{F}_A^{fr} &= \sum_{\Omega} [u(x)]^m g \left(I(x) - \left(\alpha \hat{f}_o + \beta \hat{c}_1\right)\right)^2 \\ &\quad + g \left(u_n^m - u_0^m\right) \left(I_0 - \left(\alpha \hat{f}_o + \beta \hat{c}_1\right)\right)^2 \\ &= \sum_{\Omega} [u(x)]^m g\, (I(x) - (\alpha f_o + \beta c_1))^2 \\ &\quad + \sum_{\Omega} [u(x)]^m g \left(\alpha \frac{\omega(x,y) * \Delta u_1\, (I_0 - f_o)}{\omega(x,y) * (t_1 + \Delta u_1)} \right. \\ &\quad \left. + \ \beta \frac{\Delta u_1}{t_1 + \Delta u_1} (I_0 - c_1)\right)^2 \\ &\quad - 2g \sum_{\Omega} [u(x)]^m g\, (I(x) - (\alpha f_o + \beta c_1)) \\ &\quad \left(\alpha \frac{\omega(x,y) * \Delta u_1\, (I_0 - f_o)}{\omega(x,y) * (t_1 + \Delta u_1)} + \beta \frac{\Delta u_1}{t_1 + \Delta u_1} (I_0 - c_1)\right) \\ &\quad + g \left(u_n^m - u_0^m\right) g \left(\frac{\alpha \omega(x,y) * t_1\, (I_0 - f_o)}{\omega(x,y) * (t_1 + \Delta u_1)} \right. \\ &\quad \left. + \ \frac{\beta t_1 (I_0 - c_1)}{t_1 + \Delta u_1}\right)^2 \end{aligned}$$

$$
\begin{aligned}
&= F_A^{fr} + \sum\nolimits_{\Omega} [u(x)]^m \, g \left(\alpha \frac{\omega(x,y) * \Delta u_1 \, (I_0 - f_o)}{\omega(x,y) * (t_1 + \Delta u_1)} \right. \\
&\quad \left. + \; \beta \frac{\Delta u_1}{t_1 + \Delta u_1} (I_0 - c_1) \right)^2 \\
&\quad - 2g \sum\nolimits_{\Omega} [u(x)]^m \, (I(x) - (\alpha f_o + \beta c_1)) \\
&\quad \left(\alpha \frac{\omega(x,y) * \Delta u_1 \, (I_0 - f_o)}{\omega(x,y) * (t_1 + \Delta u_1)} + \beta \frac{\Delta u_1}{t_1 + \Delta u_1} (I_0 - c_1) \right) \\
&\quad + g \Delta u_1 \left(\frac{\alpha \omega(x,y) * t_1 \, (I_0 - f_o)}{\omega(x,y) * (t_1 + \Delta u_1)} + \frac{\beta t_1 (I_0 - c_1)}{t_1 + \Delta u_1} \right)^2
\end{aligned} \tag{B-19}
$$

From (B-1) and (B-6), we have E(q. (B-1) and Eq. (B-2),

$$\sum\nolimits_{\Omega} I(x) \cdot [u(x)]^m = t_1 c_1 \tag{B-20}$$

$$\sum\nolimits_{\Omega} \omega(x,y) * \left[I(x) [u(x)]^m \right] = f_o s_1 \tag{B-21}$$

Combing (B-20), (B-21) and $\alpha + \beta = 1$, we have

$$
\begin{aligned}
\hat{F}_A^{fr} &= \sum\nolimits_{\Omega} [u(x)]^m \, g \left(\alpha \frac{\omega(x,y) * \Delta u_1 \, (I_0 - f_o)}{\omega(x,y) * (t_1 + \Delta u_1)} \right. \\
&\quad \left. + \; \beta \frac{\Delta u_1}{t_1 + \Delta u_1} (I_0 - c_1) \right)^2 \\
&\quad + g \Delta u_1 \left(\frac{\alpha \omega(x,y) * \Delta t_1 \, (I_0 - f_o)}{\omega(x,y) * (t_1 + \Delta u_1)} + \frac{\beta t_1 (I_0 - c_1)}{t_1 + \Delta u_1} \right)^2 \\
&\quad + F_A^{fr} - 2g \left(\alpha \frac{\omega(x,y) * \Delta u_1 \, (I_0 - f_o)}{\omega(x,y) * (t_1 + \Delta u_1)} \right. \\
&\quad \left. + \beta \frac{\Delta u_1}{t_1 + \Delta u_1} (I_0 - c_1) \right) \sum\nolimits_{\Omega} [u(x)]^m \, (I(x) - (\alpha f_o + \beta c_1)) \\
&= \sum\nolimits_{\Omega} [u(x)]^m \, g \left(\alpha \frac{\omega(x,y) * \Delta u_1 \, (I_0 - f_o)}{\omega(x,y) * (t_1 + \Delta u_1)} \right. \\
&\quad \left. + \; \beta \frac{\Delta u_1}{t_1 + \Delta u_1} (I_0 - c_1) \right)^2 \\
&\quad + g \Delta u_1 \left(\frac{\alpha \omega(x,y) * t_1 \, (I_0 - f_o)}{\omega(x,y) * (t_1 + \Delta u_1)} + \frac{\beta t_1 (I_0 - c_1)}{t_1 + \Delta u_1} \right)^2 \\
&\quad + F_A^{fr} - 2g \left(\alpha \frac{\omega(x,y) * \Delta u_1 \, (I_0 - f_o)}{\omega(x,y) * (t_1 + \Delta u_1)} \right. \\
&\quad \left. + \; \beta \frac{\Delta u_1}{t_1 + \Delta u_1} (I_0 - c_1) \right) \\
&\quad (\beta t_1 c_1 + \alpha f_o s_1 - (\alpha t_1 f_o + \beta t_1 c_1)) \\
&= F_A^{fr} + g t_1 \left(\alpha \frac{\omega(x,y) * \Delta u_1}{\omega(x,y) * (t_1 + \Delta u_1)} (I_0 - f_o) \right. \\
&\quad \left. + \; \beta \frac{\Delta u_1}{t_1 + \Delta u_1} (I_0 - c_1) \right)^2 \\
&\quad + g \Delta u_1 \left(\frac{\alpha \omega(x,y) * t_1}{\omega(x,y) * (t_1 + \Delta u_1)} (I_0 - f_o) \right. \\
&\quad \left. + \; \frac{\beta t_1}{t_1 + \Delta u_1} (I_0 - c_1) \right)^2
\end{aligned} \tag{B-22}
$$

Similarly, we can get

$$
\begin{aligned}
\hat{F}_B^{fr} &= g t_2 \left(\alpha \frac{\omega(x,y) * \Delta u_2}{\omega(x,y) * (t_2 + \Delta u_2)} (I_0 - f_b) \right. \\
&\quad \left. + \; \beta \frac{\Delta u_2}{t_1 + \Delta u_1} (I_0 - c_2) \right)^2 \\
&\quad + F_B^{fr} + g \Delta u_2 \left(\frac{\alpha \omega(x,y) * t_2}{\omega(x,y) * (t_2 + \Delta u_2)} (I_0 - f_b) \right. \\
&\quad \left. + \; \frac{\beta t_2}{t_2 + \Delta u_2} (I_0 - c_2) \right)^2
\end{aligned} \tag{B-23}
$$

Therefore, by inserting (B-22) and (B-23) into (B-13), we have

$$
\begin{aligned}
\hat{F}^{fr} &= F_A^{fr} + g t_1 \left(\alpha \frac{\omega(x,y) * \Delta u_1}{\omega(x,y) * (t_1 + \Delta u_1)} (I_0 - f_o) \right. \\
&\quad \left. + \; \beta \frac{\Delta u_1}{t_1 + \Delta u_1} (I_0 - c_1) \right)^2 \\
&\quad + g t_2 \left(\alpha \frac{\omega(x,y) * \Delta u_2}{\omega(x,y) * (t_2 + \Delta u_2)} (I_0 - f_b) \right. \\
&\quad \left. + \; \beta \frac{\Delta u_2}{t_1 + \Delta u_1} (I_0 - c_2) \right)^2 \\
&\quad + g \Delta u_1 \left(\frac{\alpha \omega(x,y) * t_1}{\omega(x,y) * (t_1 + \Delta u_1)} (I_0 - f_o) \right. \\
&\quad \left. + \; \frac{\beta t_1}{t_1 + \Delta u_1} (I_0 - c_1) \right)^2 \\
&\quad + F_B^{fr} + g \Delta u_2 \left(\frac{\alpha \omega(x,y) * t_2}{\omega(x,y) * (t_2 + \Delta u_2)} (I_0 - f_b) \right. \\
&\quad \left. + \; \frac{\beta t_2}{t_2 + \Delta u_2} (I_0 - c_2) \right)^2
\end{aligned} \tag{B-24}
$$

So the alteration $\Delta F^{fr} = \hat{F}^{fr} - F^{fr}$ between the new and old total energy is written as

$$
\begin{aligned}
\Delta F^{fr} &= g t_1 \left(\alpha \frac{\omega(x,y) * \Delta u_1}{\omega(x,y) * (t_1 + \Delta u_1)} (I_0 - f_o) \right. \\
&\quad \left. + \; \beta \frac{\Delta u_1}{t_1 + \Delta u_1} (I_0 - c_1) \right)^2 \\
&\quad + g t_2 \left(\alpha \frac{\omega(x,y) * \Delta u_2}{\omega(x,y) * (t_2 + \Delta u_2)} (I_0 - f_b) \right. \\
&\quad \left. + \; \beta \frac{\Delta u_2}{t_1 + \Delta u_1} (I_0 - c_2) \right)^2 \\
&\quad + g \Delta u_1 \left(\frac{\alpha \omega(x,y) * t_1}{\omega(x,y) * (t_1 + \Delta u_1)} (I_0 - f_o) \right. \\
&\quad \left. + \; \frac{\beta t_1}{t_1 + \Delta u_1} (I_0 - c_1) \right)^2 \\
&\quad + g \Delta u_2 \left(\frac{\alpha \omega(x,y) * t_2}{\omega(x,y) * (t_2 + \Delta u_2)} (I_0 - f_b) \right. \\
&\quad \left. + \; \frac{\beta t_2}{t_2 + \Delta u_2} (I_0 - c_2) \right)^2
\end{aligned} \tag{B-25}
$$

REFERENCES

[1] D. Cremers, M. Rousson, and R. Deriche, "A review of statistical approaches to level set segmentation: Integrating color, texture, motion and shape," *Int. J. Comput. Vis.*, vol. 72, no. 5, pp. 195–215, 2007.

[2] X. Muñoz, J. Freixenet, X. Cufı, and J. Martí, "Strategies for image segmentation combining region and boundary information," *Pattern Recognit.*, vol. 24, nos. 1–3, pp. 375–392, 2003.

[3] S. Kim, S. Nowozin, P. Kohli, and D. Y. Chang, "Higher-order correlation clustering for image segmentation," *IEEE Trans. Pattern Anal. Mach. Intell.*, vol. 36, pp. 1761–1774, 2015.

[4] M. Kass, A. Witkin, and D. Terzopoulos, "Snakes: Active contour models," *Int. J. Comput. Vis.*, vol. 1, no. 4, pp. 321–331, 1988.

[5] V. Caselles, R. Kimmel, and G. Sapiro, "Geodesic active contours," *Int. J. Comput. Vis.*, vol. 22, no. 1, pp. 61–79, 1997.

[6] T. F. Chan and L. A. Vese, "Active contours without edges," *IEEE Trans. Image Process.*, vol. 10, no. 2, pp. 266–277, Feb. 2001.

[7] S. C. Zhu and A. Yuille, "Region competition: Unifying snakes, region growing, and Bayes/MDL for multiband image segmentation," *IEEE Trans. Pattern Anal. Mach. Intell.*, vol. 18, no. 9, pp. 884–900, Sep. 1996.

[8] D. Mumford and J. Shah, "Optimal approximations by piecewise smooth functions and associated variational problems," *Commun. Pure Appl. Math.*, vol. 42, no. 5, pp. 577–685, 1989.

[9] C. Li, C.-Y. Kao, J. C. Gore, and Z. Ding, "Implicit active contours driven by local binary fitting energy," in *Proc. IEEE Conf. Comput. Vis. Pattern Recognit.*, Minneapolis, MN, USA, Jun. 2007, pp. 1–7.

[10] L. A. Vese and T. F. Chan, "A multiphase level set framework for image segmentation using the Mumford and Shah model," *Int. J. Comput. Vis.*, vol. 50, no. 3, pp. 271–293, Dec. 2002.

[11] C. Li, C.-Y. Kao, J. C. Gore, and Z. Ding, "Minimization of region-scalable fitting energy for image segmentation," *IEEE Trans. Image Process.*, vol. 17, no. 10, pp. 1940–1949, Oct. 2008.

[12] C. Li, C. Xu, C. Gui, and M. D. Fox, "Level set evolution without re-initialization: A new variational formulation," in *Proc. IEEE Comput. Soc. Conf. Comput. Vis. Pattern Recognit.*, San Diego, CA, USA, Jun. 2005, pp. 430–436.

[13] C. Li, C. Xu, C. Gui, and M. D. Fox, "Distance regularized level set evolution and its application to image segmentation," *IEEE Trans. Image Process.*, vol. 19, no. 12, pp. 3243–3254, Dec. 2010.

[14] K. Zhang, H. Song, and L. Zhang, "Active contours driven by local image fitting energy," *Pattern Recognit.*, vol. 43, no. 4, pp. 1199–1206, Apr. 2010.

[15] L. Wang, Y. Chang, H. Wang, Z. Wu, J. Pu, and X. Yang, "An active contour model based on local fitted images for image segmentation," *Inf. Sci.*, vols. 418–419, pp. 61–73, Dec. 2017.

[16] Z. Ji, Y. Xia, Q. Sun, G. Cao, and Q. Chen, "Active contours driven by local likelihood image fitting energy for image segmentation," *Inf. Sci.*, vol. 301, pp. 285–304, Apr. 2015.

[17] J. Miao, T.-Z. Huang, X. Zhou, Y. Wang, and J. Liu, "Image segmentation based on an active contour model of partial image restoration with local cosine fitting energy," *Inf. Sci.*, vol. 447, pp. 61–73, pp. 52–71, Jun. 2018.

[18] K. Ding, L. Xiao, and G. Weng, "Active contours driven by local pre-fitting energy for fast image segmentation," *Pattern Recogn. Lett.*, vol. 104, no. 1, pp. 29–36, Mar. 2018.

[19] X.-F. Wang, D.-S. Huang, and H. Xu, "An efficient local Chan–Vese model for image segmentation," *Pattern Recognit.*, vol. 43, no. 3, pp. 603–618, 2010.

[20] C. He, Y. Wang, and Q. Chen, "Active contours driven by weighted region-scalable fitting energy based on local entropy," *Signal Process.*, vol. 92, no. 2, pp. 587–600, Feb. 2012.

[21] T. Brox and D. Cremers, "On local region models and a statistical interpretation of the piecewise smooth Mumford-Shah functional," *Int. J. Comput. Vis.*, vol. 84, pp. 184–193, Aug. 2009.

[22] H.-J. Wang and M. Liu, "Active contours driven by local Gaussian distribution fitting energy based on local entropy," *Int. J. Pattern Recognit. Artif. Intell.*, vol. 27, no. 6, 2013, Art. no. 1355008.

[23] H. Ali, N. Badshah, K. Chen, and G. A. Khan, "A variational model with hybrid images data fitting energies for segmentation of images with intensity inhomogeneity," *Pattern Recognit.*, vol. 51, pp. 27–42, Mar. 2016.

[24] S. Krinidis and V. Chatzis, "Fuzzy energy-based active contours," *IEEE Trans. Image Process.*, vol. 18, no. 12, pp. 2747–2755, Dec. 2009.

[25] K.-K. Shyu, V.-T. Pham, T.-T. Tran, and P.-L. Lee, "Global and local fuzzy energy-based active contours for image segmentation," *Nonlinear Dyn.*, vol. 67, no. 2, pp. 1559–1578, 2012.

[26] A. Mondal, S. Ghosh, and A. Ghosh, "Robust global and local fuzzy energy based active contour for image segmentation," *Appl. Soft Comput.*, vol. 47, pp. 191–215, Oct. 2016.

[27] A. Mondal, S. Ghosh, and A. Ghosh, "Partially camouflaged object tracking using modified probabilistic neural network and fuzzy energy based active contour," *Int. J. Comput. Vis.*, vol. 122, no. 1, pp. 116–148, 2017.

[28] W. Sun, E. Dong, and H. Qiao, "A fuzzy energy-based active contour model with adaptive contrast constraint for local segmentation," *Signal, Image Video Process.*, vol. 12, no. 1, pp. 91–98, 2018.

[29] T.-T. Tran, V.-T. Pham, and K.-K. Shyu, "Image segmentation using fuzzy energy-based active contour with shape prior," *J. Vis. Commun. Image Represent.*, vol. 25, no. 7, pp. 1732–1745, 2014.

[30] K. Zhang, L. Zhang, H. Song, and W. Zhou, "Active contours with selective local or global segmentation: A new formulation and level set method," *Image Vis. Comput.*, vol. 28, no. 4, pp. 668–676, 2010.

[31] H. Zhang, J. E. Fritts, and S. A. Goldman, "An entropy-based objective evaluation method for image segmentation," *Proc. SPIE*, vol. 5307, pp. 38–49, Dec. 2003.

[32] T. Liu *et al.*, "Learning to detect a salient object," *IEEE Trans. Pattern Anal. Mach. Intell.*, vol. 33, no. 2, pp. 353–367, Feb. 2011.

[33] M. B. Salah, A. Mitiche, and I. B. Ayed, "Effective level set image segmentation with a kernel induced data term," *IEEE Trans. Image Process.*, vol. 19, no. 1, pp. 220–232, Jan. 2010.

JIANGXIONG FANG received the B.S. and M.S. degrees from Central South University, Changsha, China, in 2004 and 2007, respectively, and the Ph.D. degree in pattern recognition and intelligent systems from the Institute of Image Processing and Pattern Recognition, Shanghai Jiao Tong University, Shanghai, China, in 2012. He is currently an Associate Professor as a Teacher with the East China University of Technology. His research interests include image segmentation and machine learning.

HUAXIANG LIU received the B.S. and M.S. degrees in circuits and systems from Hunan Normal University, in 2007 and 2010, respectively. She is currently a Teacher with the East China University of Technology. Her research interests include remote sensing image processing, convex optimization problem, variational theory for image segmentation, and visual object tracking and detection.

LITING ZHANG received the B.S. degree from the Hefei University of Technology, Hefei, in 1999, the M.S. degree from the East China of Technology, Fuzhou, China, in 1990, and the Ph.D. degree in cartography and geographic information engineering from Wuhan University, Wuhan, China, in 2006. His research interests include remote image processing and GIS theory and application.

JUN LIU received the B.S. and M.S. degrees from the Shenyang University of Technology, Shenyang, in 2003 and 2006, respectively, and the Ph.D. degree in detection technology and automation devices from Northeastern University, Shenyang, China, in 2010. He is currently an Associate Professor as a Teacher with the East China University of Technology. His research interests include metallurgical parameters detection and image processing.

HESHENG LIU received the B.S., M.S., and Ph.D. degrees from Shanghai Jiao Tong University, Shanghai, China. He was selected as the New Century National Hundred, Thousand and Ten Thousand Talent Project in China and Special allowance of the State Council. He is currently a Professor, and is serving as the President of the East China University of Technology. His research interests include mechanical and electrical integration, advanced control systems, and optimization algorithm.